The Rich Polymorphism of Layered NbS_3

Sergio Conejeros,[†] Bogdan Guster,[‡] Pere Alemany,[¶] Jean-Paul Pouget,[§] and Enric Canadell[*,‖]

†*Departamento de Química, Universidad Católica del Norte, Av. Angamos 0610, Antofagasta 1240000, Chile*

‡*Institute of Condensed Matter and Nanosciences, Université Catholique de Louvain, Chemin des étoiles 8, B-1348 Louvain-la-Neuve, Belgium*

¶*Departament de Ciència de Materials i Química Física and Institut de Química Teòrica i Computacional (IQTCUB), Universitat de Barcelona, Martí i Franqués 1, 08028 Barcelona, Spain*

§*Laboratoire de Physique des Solides, CNRS UMR 8502, Université de Paris-Sud, Universié Paris-Saclay, 91405 Orsay, France*

‖*Institut de Ciència de Materials de Barcelona, ICMAB-CSIC, Campus UAB, 08193 Bellaterra, Spain*

E-mail: canadell@icmab.es

Abstract

Layered group V transition metal trichalcogenides are paradigmatic low-dimensional materials providing an ever increasing series of unusual properties. They are all based on the same basic building units, one-dimensional MX_3 (M= Nb, Ta; X= S, Se) trigonal-prismatic chains that condense into layers, but their electronic structures exhibit significant differences leading to a broad spectrum of transport properties, ranging from metals with one, two, or three charge density wave instabilities to semimetals with

potential topological properties or semiconductors. The different physical and chemical properties are shown to be related with subtle structural differences within the layers that result in half-, third-, or quarter-filled quasi-one-dimensional Nb d_{z^2}-type bands, providing a clear-cut illustration of the intimate link between structural and electronic features within a family of solids. An interesting yet not sufficiently explored feature of these solids is the polymorphism. Based on both experimental and new theoretical results we examine this aspect for NbS_3 and show that at least seven different polymorphs with a stability compatible with the presently known phases of this compound are possible. We discuss a simple rationale for the physical properties of the presently known polymorphs, as well as predictions for those that have still not been characterized or prepared. It is argued that some of the presently unknown polymorphs may have been prepared in an uncontrolled way as mixtures of different phases which could not be structurally characterized. The rich landscape of structures and properties found for this van der Waals material is suggested to represent an ideal platform for the preparation of flakes with fine-tuned properties for applications in new electronic and optoelectronic devices.

Introduction

Layered group V transition metal trichalcogenides display a plethora of challenging physical and chemical properties such as charge density waves (CDW), superconductivity, easy chemical intercalation, etc.[1] Very recently it has been shown that they may also provide useful platforms for next generation electronic and optoelectronic 2D materials.[2,3] The CDW material $NbSe_3$ for instance is one of the archetypal systems in low-dimensional materials science.[4,5] It was the first inorganic solid found to exhibit Fröhlich type conductivity and this observation launched a huge and continued interest on it. Almost forty years later, very fundamental aspects of its physical and chemical behavior still remain challenging.[6–9] $NbSe_3$[10,11] is a room temperature quasi one-dimensional metal[12] which undergoes two successive Fermi

surface driven incommensurate CDW transitions at 145 K and 59 K, respectively.[11,13,14] After the second CDW transition $NbSe_3$ still exhibits metallic character, so that the Fermi surface is not completely removed by the CDWs. Interestingly, monoclinic-TaS_3 (m-TaS_3)[15] which is isostructural with $NbSe_3$ and exhibits also two successive incommensurate CDWs at 240 K and 160 K[16] becomes semiconducting after the second transition, indicating that the Fermi surface has been indeed completely destroyed in this case. Such contrasting low temperature behavior has been related to the different strength of the inter-chain interactions.[9,17]

The crystal structure of $NbSe_3$,[11] as those of all systems to be discussed in this work, is built from a series of MX_3 chains where the transition metal atoms are in a trigonal prismatic coordination (see Fig. 1a). It may be considered as a less symmetric variation of the TiS_3 type structure[18] (Fig. 1b). While all trigonal prismatic chains are structurally equivalent in the TiS_3 structure, three non equivalent chains, marked as I, II, and III in Fig. 1a, can be distinguished in the $NbSe_3$ structure. The high symmetry TiS_3 type structure has been found for all group IV MX_3 solids (M= Ti, Zr, Hf; X= S, Se, Te). It is important to note that since in this type of structures two adjacent chains are displaced by half the repeat vector along the chain direction (b), the transition metal atom is actually coordinated to six X atoms of its own chain *and* two additional X atoms of the neighboring chains, leading to an MX_3 layer. A very important structural observation is that in the group IV MX_3 phases the X_3 triangles are not equilateral-like but isosceles since one of the X-X contacts, highlighted in green in Fig. 1b, is compatible with an X-X bond, whereas the other two are equivalent, but considerably longer. Thus, for electron counting purposes the isolated X atoms must be considered as X^{2-} and the X-X bonded pair as $(X_2)^{2-}$, leaving the transition metal atom as d^0. For group V MX_3 compounds, the additional electron per transition metal atom leads to two significant structural changes that strongly affect the electronic structure. First, as a result of the additional electrons, some X-X bonds are broken and the X_3 triangles become almost equilateral (see the chains labelled II in Fig. 1a where the broken bond has been shown as a dashed line). Second, as a consequence of the local strain generated by the

increased X-X distance, the layer rearranges at this region and one pair of trigonal prismatic chains is tilted with respect to the layer horizontal c axis (see chains III in Fig. 1a).

What these simple structural observations are telling us is that *the extra electron provided by the transition metal atom in group V trichalcogenides may be used to induce either (i) metal-metal bonding (i.e. commensurate or incommensurate CDW or Peierls distortions) or (ii) S-S bond reduction (i.e. formation of equilateral-type chains).* The ratio between the number of electrons used in the two processes will impose the shape of the trigonal prismatic based layers and subtly change the d^x ($0< x <1$) electron count of the transition metal atoms and consequently, the electronic structure and properties of the solid. This observation immediately suggests that group V trichalcogenides should be prone to occur in several polymorphic forms (here we are mostly interested in polymorphic forms with different types of layers because, as it will be seen, polymorphs due to different layer stacking do not change the transition metal electron count and thus, have little effect on the transport properties) with different properties and that the presently known systems may well be just the tip of the iceberg.

Different polymorphic forms were in fact early observed for some of these solids. For instance, TaS_3 occurs in orthorhombic and monoclinic structures differing in their layer packing.[1,16] For a long time the only crystal structure known for NbS_3 (labelled as NbS_3-I from now on)[20] was based on the TiS_3 one (Fig. 1b). Since in this structure all S_3 triangles are isosceles, the Nb atoms are thus formally d^1. The observation of a semiconducting behavior, together with a doubling of the periodicity along the chain direction, where Nb-Nb short and long distances alternate, was considered as the result of a Peierls transition due to the occurrence of a formally half-filled band that opens a band gap at the Fermi level. However, it has been recently shown that a metallic state is induced under pressure[21] and thermoelectric power measurements suggest that NbS_3-I is not a usual Peierls distorted system.[22] The existence of a second polymorph, NbS_3-II, has also been known for longtime.[1] Although different superstructures of the basic NbS_3-I structure were proposed for this polymorph,

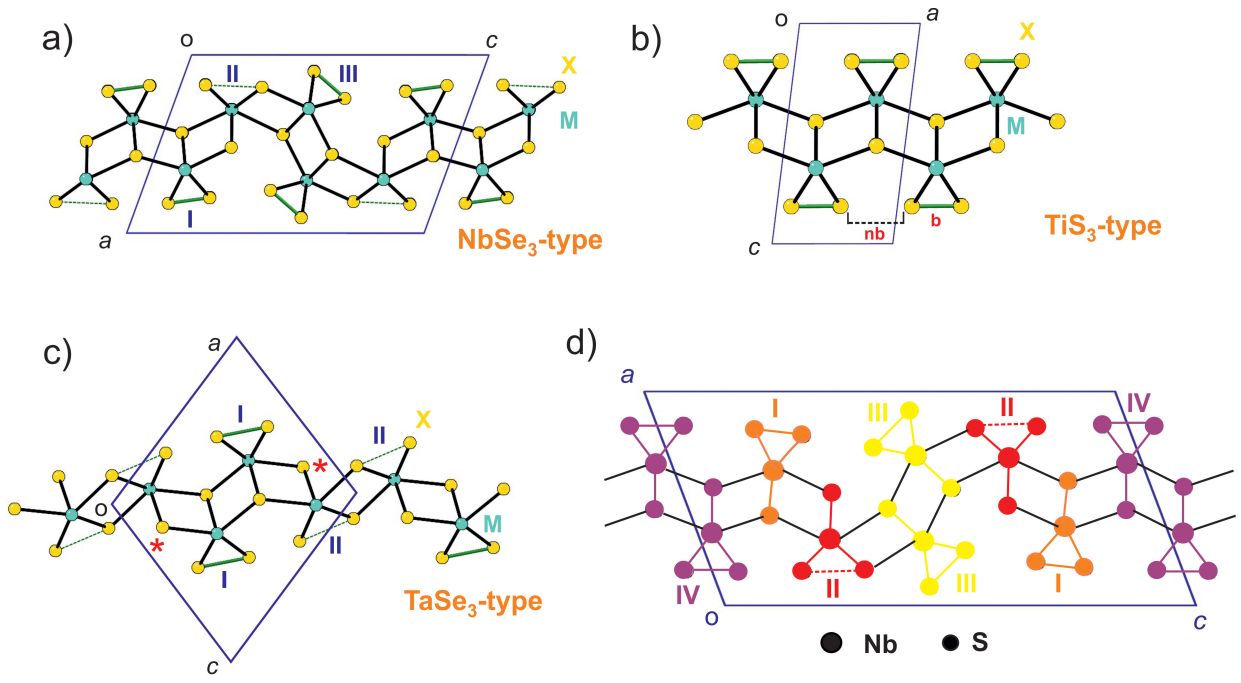

Figure 1: Top view of different MX_3 crystal structures: (a) $NbSe_3$/*m*-TaS_3, (b) TiS_3, (c) $TaSe_3$ and (d) NbS_3-II. In all cases adjacent chains are shifted by 1/2 the repeat vector along the chain direction (i.e. *b*). In (a), (b) and (c) the short and relatively long X...X contacts important for electron counting are shown as full and dashed green lines, respectively. The labels I, II, III and IV denote different trigonal prismatic chains (see text). In (d) the four different types of chains are shown with different colors using the same color coding as in the experimental structural determination.[19] The short and relatively long X...X contacts are shown as full and dashed lines, respectively. By analogy with $NbSe_3$ (a), the chain with a long S...S triangular side is labeled as chain II and the chain which is tilted with respect to the *c*-direction of the layer will be refereed to as chain III.

a clear-cut structural determination remained elusive until recently (Fig. 1d).[19] NbS_3-II is metallic[23] and has been reported to exhibit three CDWs at around 450-475 K, 360 K and 150 K, respectively.[24] This behavior is reminiscent of the $NbSe_3$ and *m*-TaS_3 systems, but now with an additional CDW transition. In fact, the situation is considerably more complex. The existence of two additional polymorphs, NbS_3-III [25] and NbS_3-HP (obtained under pressure),[26] has been reported but their crystal structures are not known. It has been suggested that NbS_3-III, which exhibits a CDW transition at 155 K,[25] may be a sub-phase of NbS_3-II.[24]

Very recently, the crystal structure of two additional phases, NbS_3-IV and NbS_3-V, was reported.[27] NbS_3-IV is essentially the NbS_3-I phase with a doubling of the cell along the inter-layer direction. The NbS_3-V structure is, however, quite different. It is essentially that of NbS_3-I *without* the doubling along the chain direction, i.e. really a TiS_3-type structure. Consequently, this phase is expected to be metallic, although this aspect has not been studied in any detail yet. However it is worth pointing that, although a full structural characterization was not possible, Izumi *et al.* reported[28] the preparation of NbS_3 samples without a doubling of the *b* cell parameter which are metallic and even superconducting at 2.15 K.

Since metallic MX_3 phases of group V (M= Nb, Ta; X= S, Se) elements have been at the origin of some of the more celebrated discoveries in low-dimensional materials science[1,4] these results bring to the fore the need for further attention to the polymorphism of these materials. This is all the more interesting in view of the recent interest on MX_3 systems as single- or few-layer systems with promising applications in electronic and optical devices as a result of their very anisotropic electronic structure.[2,29–32] In fact, nanoribbons of both NbS_3-I and $NbSe_3$,[33] nanofibers of TaS_3 ,[34] microwires of $TaSe_3$[35,36] and single-layer $TaSe_3$ nanoribbons on SiO_2/Si substrates[37] have already been reported.

Our purpose here is to point out that numerous polymorphs associated with different physical and chemical behaviour, some of which not yet prepared or characterized, are pos-

sible because of the intimate connection between the S-S bond reduction and metal-metal bonding abilities of these layers. We will emphasize the subtle link between structural and electronic features on the basis of recent experimental results and new theoretical data. To illustrate our claim we will consider in some detail the case of NbS_3 and we will provide a rationale for recent experimental results on the new polymorphs. Similar ideas should apply to the other M/X combinations.

Results and Discussion

Stability of different NbS_3 polymorphs

Since the available experimental information suggests a rich polymorphism for NbS_3 we first carried out a DFT study of different NbS_3 polymorphs (see the Supplementary Information (SI) for details of the calculations). We were able to locate seven different polymorphs with a fully optimized structure. The calculated cell parameters, relative energy and band gaps are reported in Table 1. One of them is the well known NbS_3-I phase,[20] three correspond to the recently characterized NbS_3-II,[19] NbS_3-IV[27] and NbS_3-V[27] phases and the remaining three are so-far unreported polymorphs with the structures of $NbSe_3$, TiS_3 and $TaSe_3$, respectively. The agreement between experimental and theoretical structures for the four presently characterized compounds is excellent thus lending reliability to these calculations.

Table 1: Calculated cell parameters, band gap and relative stability for different NbS_3 polymorphs using the HSE06 functional (see SI for details). The errors with respect to the experimental cell constants for polymorphs whose structure has been determined are given in parenthesis.

	NbS_3-I	NbS_3-IV	"$NbSe_3$"	NbS_3-II	"$TaSe_3$"	NbS_3-V'	NbS_3-V
a/Å	4.967 (0.1%)	6.746 (-0.1%)	9.692	9.714 (0.6%)	10.278	4.828	4.944 (-0.1%)
b/Å	6.745 (0.2%)	4.967 (-0.1%)	3.356	3.352 (0.2%)	3.392	3.346	3.340 (-0.5%)
c/Å	9.215 (0.8%)	18.277 (0.8%)	14.680	19.551 (-1.5%)	9.253	9.113	9.254 (1.9%)
β/°	97.21 (-0.1%)	90.21 (0.1%)	108.64	108.73 (-1.8%)	109.51	81.79	96.63 (-0.7%)
$V(f.u.)$/Å^3	76.570 (1.1%)	76.548 (0.6%)	75.415	75.360 (0.5%)	76.030	72.860	75.885 (1.4%)
Band gap (eV)	0.91	1.06	Metallic	Metallic	0.33	Metallic	Metallic
Rel. Energy (meV)/NbS_3	0.0	0.49	46.9	47.7	118.4	198.7	211.1

The labelling used all along this work to designate the different polymorphs is the following: (1) **NbS_3-I**: the semiconducting system with crystal structure determined by Rijnsdorf and Jellinek[20] exhibiting two trigonal prismatic chains in the unit cell with an alternation of short and long Nb-Nb distances (Fig. 1b with periodicity doubled along b), (2) **NbS_3-II**: the polymorph exhibiting three CDWs whose crystal structure has been recently reported[19] (see Fig. 1d), (3) **"$NbSe_3$"-type**: the hypothetical phase exhibiting the $NbSe_3$[10,11] or m-TaS_3[15] crystal structure (Fig. 1a), (4) **"$TaSe_3$"-type**: the hypothetical phase exhibiting the $TaSe_3$ structure type[38] (Fig. 1c), (5) **NbS_3-IV**: the structure[27] closely resembling NbS_3-I, i.e. with dimerized trigonal prismatic chains, but containing two symmetry related layers per unit cell, (6) **NbS_3-V**: the recently reported structure[27] exhibiting the same structure as NbS_3-I *without* the doubling along the direction of the chains, i.e., the structure of TiS_3 (Fig. 1b), and (7) **NbS_3-V'**: another hypothetical structure very close to NbS_3-V, but with a variation in the sulfur sublattice.

The main results emerging from this study are the following:

(1) The NbS_3-I structure, which for a longtime was the only structurally well characterized polymorph, is found to be the lowest energy phase. The recently reported NbS_3-IV polymorph is, however, only marginally less stable as expected from the fact that the intralayer structure is practically identical to that of NbS_3-I and only the layer stacking differs between both structures (see Figure S5 in SI).

(2) A pair of polymorphs, NbS_3-II and "$NbSe_3$"-type, with different structure but very small energy difference are the next more stable phases. This is a very appealing result because NbS_3-II exists and it is now well characterized so that there are all the reasons to think that the so-called "$NbSe_3$"-type structure may actually exist. In fact, the two phases are but two members of a structural family (see Figs 1a and 1d). As it will be discussed later, in both phases one pair of trigonal prismatic chains (type II) has the short S-S side of the sulfur triangles too long to be considered a single bond. Thus, the two phases have a different number of chains with short S-S contacts compatible with a single S-S bond (two pairs -types

I and III- in the "$NbSe_3$"-type phase and three pairs -types I, III and IV- in NbS_3-II) and the same number of chains without an S-S bond (one type II pair). Consequently both phases should be low-dimensional metals but with a different filling of the partially filled bands. This raises the possibility of changing the number and nature of the modulation of the CDWs for these structurally related polymorphs.

(3) The next more stable polymorph ("$TaSe_3$"-type) exhibits a structure similar to $TaSe_3$ (see Fig. 1c), with one pair of chains per unit cell where the short S-S side is compatible with a single bond and another pair of chains where it is not. Thus, in a certain sense, it can be considered as the first member of the previously mentioned family even if there are some subtle differences in the crystal structure.

(4) The less stable polymorphs that we have been able to locate are NbS_3-V and NbS_3-V'. Both structures correspond to the popular TiS_3 structural type *without* the doubling along the chains direction. The two structures somewhat differ in the sulfur sublattice and both contain just one layer per unit cell. One of them, NbS_3-V, has been recently reported as a stable polymorph[27] thus providing support to the potential existence of all other so far unknown polymorphs of Table 1.

NbS_3-II: CDWs in a polymorph with average one-third filled Nb d_{z^2} bands

Links between the crystal and electronic structure

The NbS_3-II polymorph is the first reported low-dimensional system exhibiting three different CDWs. In this section we will consider the link between the crystal and electronic structures of this material in order to understand the origin and mechanism of these CDW instabilities. The unit cell of NbS_3-II contains eight chains of Nb atoms trigonally coordinated with S atoms running along the b-direction (Fig. 1d). There are four different types of NbS_3 chains which in order to simplify the discussion have been highlighted with different colors in Fig. 1d

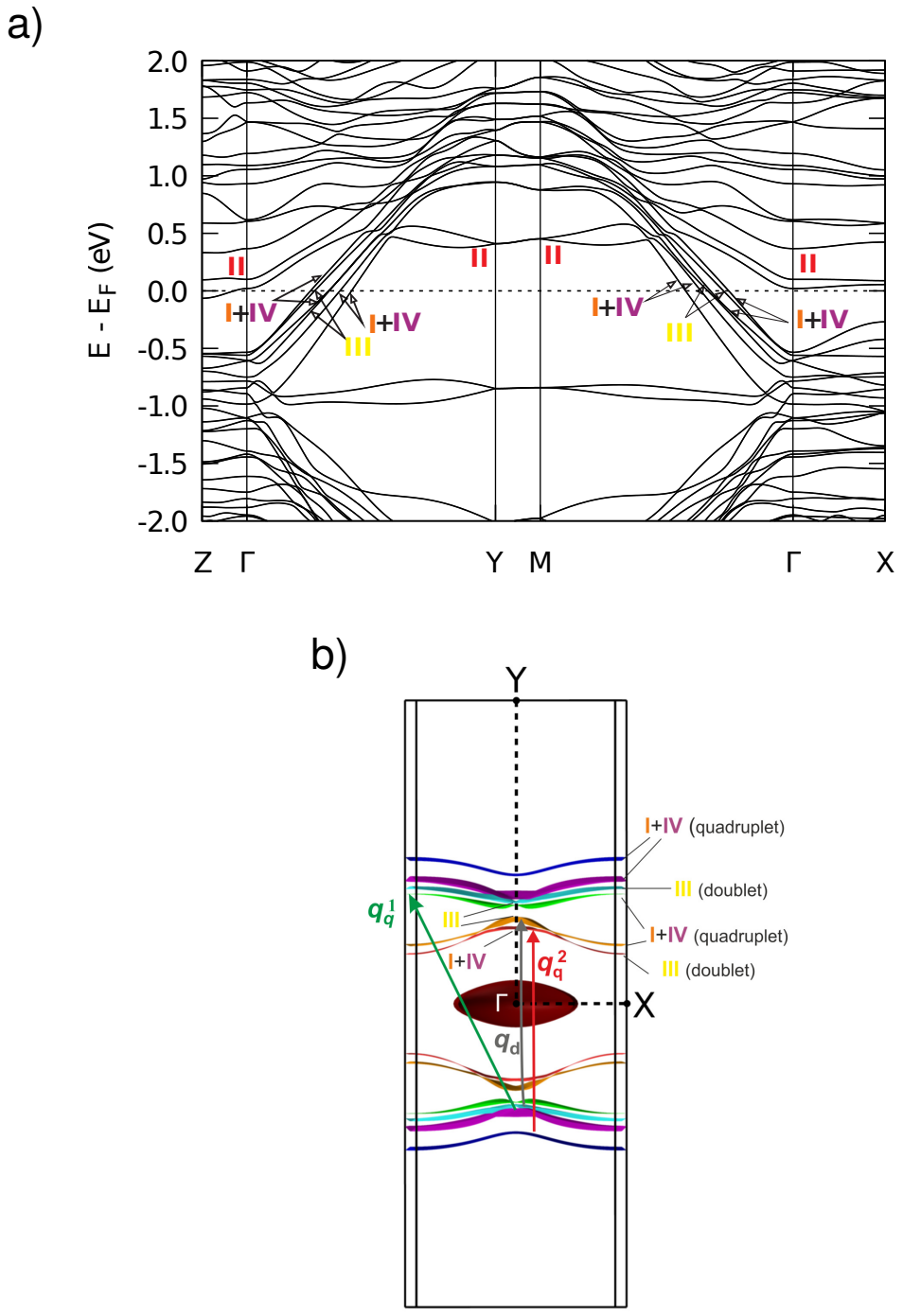

Figure 2: (a) Band structure of NbS_3-II calculated using the experimental crystal structure and the PBE functional. Γ= (0, 0, 0), X= (1/2, 0, 0), Y= (0, 1/2, 0), M= (0, 1/2, 1/2) and Z=(0, 0, 1/2) in units of the monoclinic reciprocal lattice vectors. The chains associated with the different partially filled bands near the Fermi level are labelled with the corresponding roman numbers (see also Figure S3 in SI). (b) Fermi surface calculated for NbS_3-II. The different colors are only a help to the view and are unrelated to the colors associated with the different chains. The doublet (chains III) or quadruplet (chains I+IV) character of the FS sheets is shown. Three nesting vectors relevant for the discussion are shown.

(to help the comparison with experimental results, these colors are the same as in the recent structural determination of the average structure[19]). The purple and yellow chains are paired in respective dimer units whereas the red and orange chains form mixed red-orange pairs. The purple, yellow and orange chains contain one short S-S triangular side, compatible with an S-S bond (2.208, 2.241 and 2.040 Å in the experimental structure, i.e. the purple, yellow and orange S-S bonds shown in Fig. 1d, respectively). However, in the red chains such distance is too long (2.582 Å) to be associated with an S-S bond. We remind that because of the displacement of adjacent chains by half the repeat vector along the chain direction, every transition metal atom is eight-coordinated (a triangular prism formed by six S atoms of its own chain with two additional S atoms of the neighboring chains capping two rectangular faces) thus leading to (*bc*) NbS_3 layers. There are several S...S contacts, both intra-layer (some being as short as 2.562, 2.752, 2.954 Å,...) and inter-layer (3.269, 3.422, 3.475 Å,...), shorter than twice the van der Waals radii of sulfur (i.e. 3.6 Å) thus conferring some 3D character to the whole system.

Since for electron counting purposes the isolated S atoms must be considered as S^{2-} and those involved in S-S bonds as $(S_2)^{2-}$, the purple, yellow and orange chains can be described as $[Nb(S^{2-})(S_2^{2-})]$ and the red chains as $[Nb(S^{2-})_3]$. Thus, using the simplified notation for the chains defined in Fig. 1d, NbS_3-II can be electronically described as $2 \times [Nb_I(S^{2-})(S_2^{2-}) + Nb_{II}(S^{2-})_3 + Nb_{III}(S^{2-})(S_2^{2-}) + Nb_{IV}(S^{2-})(S_2^{2-})]$. This leaves just four electrons to fill the low-lying bands of eight NbS_3 chains. Since the Nb atoms of chains II are formally d^0 the four electrons will fill the low-lying bands of chains I, III and IV. For a transition metal atom in a trigonal prismatic coordination there are three low-lying d orbitals. However, as it has been described in detail elsewhere,[9,17,39] because of the actual eight-fold coordination, two of these orbitals are pushed to high energies and only the Nb d_{z^2} orbitals, with z in the direction of the chains, remain low in energy. Consequently, there are just four electrons to fill the six low-lying bands of NbS_3-II which, on the basis of these qualitative ideas, should be based on the d_{z^2}-type orbitals of the Nb atoms in chains I, III and IV. This leads to a set

of six one-third-filled d_{z^2}-type bands.

The band structure around the Fermi level calculated using the experimental crystal structure and the PBE functional is shown in Fig. 2a (to facilitate the comparison with some previous works we use the labeling of special points in the BZ shown in Fig. S1 of the SI) together with a fatband analysis of the bands in Fig. S3 of the SI (all along this work we use a local system of axes to describe the orbitals centered at the Nb atom under discussion with the z axis along the trigonal prismatic chains and the x axis along the inter-chain direction within the layers). The bands calculated using the PBE functional for the optimized structure lead to the same conclusions (see the discussion below and Fig. S2 in SI). In agreement with the qualitative analysis there are six dispersive and partially filled bands with an average filling of one-third which should confer metallic properties to this polymorph. As expected, these bands are strongly based on the Nb d_{z^2}-type orbitals. Two of the six dispersive partially filled bands, the third and fifth bands at the Fermi level when going from Y to Γ, noted III (yellow) in Fig. 2a, are located almost exclusively on the yellow $Nb_{III}S_6$ chains (see Fig. S3(a) of the SI). The other four bands, noted I (orange)+ IV (purple) in Fig. 2a, have mixed character of the orange (Nb_IS_6) and purple ($Nb_{IV}S_6$) chains (see Fig. S3 of the SI). Although along some lines of the BZ one of the two types of chains may seem to predominate, this is not the case because the predominant chain character varies along the BZ and the mixing is strong. The interaction between the purple and orange chains is mediated by an S...S contact linking directly the two S-S bonds of the respective chains which is considerably shorter than twice the van der Waals radius of sulfur (3.012 vs. 3.60 Å). Thus, from an electronic viewpoint the two purple and two orange chains should be collectively considered as a quadruplet. In short, at the Fermi level two bands are strongly localized on the tilted pair of yellow chains and the remaining four in the quadruplet of purple and orange chains. The bands based on the red $Nb_{II}S_6$ chains, i.e. the bands noted II (red) in Fig. 2a, on the contrary, are above the Fermi level for most of the Brillouin zone (Fig. S3(b) of the SI). One of the two bands of this type cuts the Fermi level only around the

Z point leading to a small closed pocket in the Fermi surface. Consequently, despite their weak contribution to the metallic character, the red $Nb_{II}S_6$ chains should not be primarily affected by the formation of CDWs in the system. Although one should properly distinguish between oxidation states and atomic populations note that, in agreement with the formal oxidation states, the calculated Mulliken gross atomic populations of Nb atoms in chains without short S...S bonds are smaller ($\sim$ 4.6) than those of the Nb atoms in chains with a short S...S bond ($\sim$ 4.7-4.8), for all polymorphs considered in this work.

The two bands based on the tilted yellow chains are not degenerate around the Fermi level, in contrast with the situation in $NbSe_3$.[7–9] In addition, the separation between the full set of dispersive, partially filled bands is larger here than in $NbSe_3$.[9] Both facts evidence strong inter-chain interactions, in fact stronger than in the selenium based $NbSe_3$, particularly when taking into account that sulfur atoms have less diffuse p orbitals. For instance, the inter-chain interactions in sulfur based m-TaS_3 are clearly weaker than in $NbSe_3$ according to similar DFT calculations.[9] However, the inter-chain interactions occur essentially through the inter-layer a-direction since the dispersion associated with these bands is very small along the c*-direction (see Γ-Z in Fig. 2a) but quite significant along the a*-direction (see Γ-X in Fig. 2a). Such inter-layer inter-chain interactions are quite significant for the yellow type III chains (see the Γ-X direction in Fig. S3(a) of the SI. The chains of the quadruplet also interact, even if a bit less, mostly due to inter-layer contacts of the purple type-IV chains (see the Γ-X direction in Fig. S3(c) of the SI. The dispersion along the inter-chain intra-layer c-direction is hampered by two structural features: (i) the long S...S distance (2.582 Å; dotted red line in Fig. 1d) in the red chains which raises the energy of the Nb d_{z^2} orbitals of the red chains thus decoupling the quadruplet and doublet Nb d_{z^2}-based bands, and (ii) the tilting of the yellow chains which leads to unfavourable S...S interactions between the orange and yellow chains.

Nature of the Fermi surface

The calculated Fermi surface is shown in Fig. 2(b). As expected, there are six pairs of sheets associated with (i) the quadruplet of purple and orange chains and (ii) the doublet of yellow chains, with an additional closed pocket related to the red chains. Note that this closed pocket is not centered at the Γ point as it could be suggested by the view in Fig. 2(b) but at the Z point of the BZ (see Fig. S4 in the SI). The six pairs of sheets are somewhat warped along the a^*-direction whereas there is no warping at all along the c^*-direction because of the nature of the inter-chain contacts discussed in the previous subsection. The warping of these sheets is intermediate between those calculated with the same computational settings for the related $NbSe_3$ and m-TaS_3 phases.[9] Since there are some avoided crossings between the FS sheets, we have included some labels to indicate the nature of the chains associated with the different sheets in order to facilitate the discussion. Note that the pair of FS sheets closer to Γ, one of the sheets being associated with the pair of yellow chains and the other with the quadruplet, interchange character along a^* because of a very weakly avoided crossing as a result of the slightly larger inter-chain inter-layer interactions of the yellow chains. However, the fact that the crossing is very weakly avoided makes it clear that there is a substantial decoupling of the quadruplet and yellow chains as far as the electronic structure around the Fermi level is concerned.

The sheets of the FS in Fig. 2(b) exhibit several nesting vectors, q. In order to see if some of them may be relevant to understand the origin of the CDWs in NbS_3-II we have calculated the Lindhard response function (Eq. 1 in SI). Four different scans of the ($0a^*$, q, $0c^*$), ($0a^*$, q, $0.5c^*$), ($0.5a^*$, q, $0c^*$), ($0.5a^*$, q, $0.5c^*$) Lindhard response at 5 K are shown in Fig. 3. For a given value of the a^* component the scans corresponding to the $0c^*$ and $0.5c^*$ components practically superpose so that only two of the scans are actually visible in the figure. Although these scans are quite *noisy* because of the occurrence of many inter-chain nestings which would be irrelevant under inclusion of the $|< i,k \mid \exp(iqr) \mid j,k+q >|^2$ matrix elements in the numerator of the Lindhard response function,[40] there are three well defined

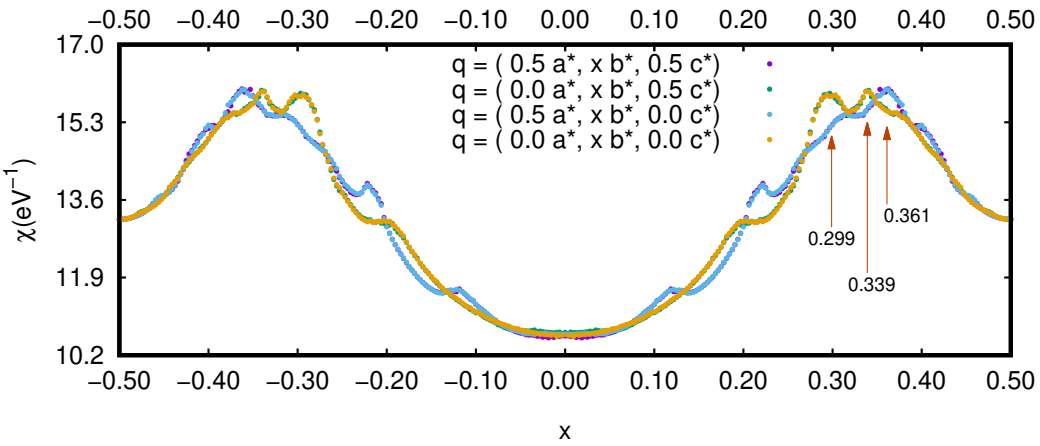

Figure 3: Four scans of the Lindhard response function calculated for NbS_3 at 5K. Note that for a given value of the a^* component the scans corresponding to the $0c^*$ and $0.5c^*$ components practically superpose so that only two scans are actually visible.

maxima with b^* components matching very well the experimental ones. These maxima of the response occur for the a^*/b^* components 0.5/0.361, 0/0.299 and 0/0.339, respectively. The first maximum corresponds to the vector nesting two quadruplet based sheets, q_q^1 in Fig. 2(b). If the very weakly avoided crossing between the pair of warped sheets near to Γ is disregarded, the second maximum corresponds to the vector nesting pairs of doublet based sheets, q_d in Fig. 2(b). Finally, the third maximum corresponds to the vector nesting the two remaining quadruplet based sheets, q_q^2 in Fig. 2(b). Consequently, two intra-quadruplet nesting vectors, q_q^1 and q_q^2, and one intra-doublet one, q_d, can destroy most of the Fermi surface of NbS_3-II upon the onset of the corresponding CDWs.

Origin of the CDW

NbS_3-II has been reported to exist in two different subphases, the so-called low-ohmic and high-ohmic phases with different conductivities and most likely with slightly different stoichiometries (i.e. some sulfur vacancies in the more conducting low-ohmic phase).[41,42] The first subphase is prepared at 670-700 °C and the second one at 715-740 °C. At around 800 K the high-ohmic phase converts into the low-ohmic one.[24] Both subphases exhibit two high-temperature CDWs at $T_{P0} \approx$ 450-475 K and T_{P1}=360 K.[23,24,43,44] The transition at

T_{P1} is clearly detected in transport and structural studies.[23,24,44] The associated q_1= (0.5a*, 0.298b*, 0) satellites,[23,43] decrease noticeably above 350 K[23] and at higher temperatures only the q_0= (0.5a*, 0.352b*, 0) satellites remain detectable up to around 450 K.[23] The low-ohmic phase exhibits a third CDW at T_{P2}= 150 K which is clearly detected in the resistivity curves.[24] However, x-ray and electron diffraction experiments were unsuccessful in providing evidence of structural changes. Remarkably, it has been reported that nonlinear conduction due to the sliding of the CDW occur for the three CDWs.[23,42]

The DFT calculation clearly points out the possibility of three different FS instabilities that would successively destroy most of the six FS sheets. The experimental wave vector of the highest temperature CDW, q_0= (0.5a*, 0.352b*, 0), is in nice agreement with one of the calculated FS nesting vectors, q_q^1= (0.5a*, 0.361b*, 0). We thus suggest that the 450-475 K CDW originates from a Fermi surface instability associated with the quadruplets of purple and orange chains. Note that although the number of charge carriers associated with the chains of the quadruplet must have decreased considerably as a consequence of this CDW, the quadruplet still sustains a metallic character for temperatures below this transition because of the two remaining pairs of quadruplet based FS sheets.

After this transition, four of the six nested pairs of FS sheets still remain and thus the possibility for the occurrence of two more CDWs persists. The two instabilities are associated with either the yellow doublets or the quadruplets. The perfect match between the intra-chain components of the experimental modulation wave-vector (0.298b*) and the calculated q_d nesting vector of Fig. 2(b) (0.299b*) strongly suggests that the second CDW originates from the doublet of yellow chains and more particularly, from the niobium atoms of these chains. The 1/2a* component in the experimental modulation is most likely a consequence of the already existing doubling of the periodicity along the inter-layer direction as a consequence of the higher temperature CDW. Our results and proposal disagree with the discussion of Zupanič et al.[19] which, in the process of putting forward different models for the CDW structural modulations, argued that only the sulfur atoms were affected by

such modulations, leaving the niobium atoms in their equilibrium positions. In addition, the displacements of the sulfur atoms were confined into the (010) planes (i.e. perpendicular to the chains). Based on well-known experimental facts for compounds of this family we have real concerns about the appropriateness of these structural features. First, NbS_3-I, the well known semiconducting structure with doubled periodicity along the chains exhibits a strong ..Nb-Nb...Nb-Nb.. alternation along the chain direction.[20] Second, the transition metal atoms in the CDW modulated structures of $NbSe_3$ and m-TaS_3 are those more strongly affected by the modulation[11,13,14,16,45] and their displacement is mostly in the chain direction. Third, a large number of physical measurements (NMR, X-ray scattering, etc.; see a review in[4]) on the latter systems can only be understood on the basis of strong and dominant displacements of the transition metal atoms. In addition, most of these data have been conveniently rationalized on the basis of DFT calculations similar to those reported here.[7–9,46] We thus firmly suggest that the second CDW occurring near room temperature is associated with niobium displacements along the chain direction of the doublet of yellow chains.

After the second CDW transition, two pairs of nested FS sheets associated with the quadruplets still remain. Thus we are tempted to associate the third CDW with the q_q^2 nesting which will destroy these quadruplet based sheets. Note that the structural modulation associated with the first CDW must have already modified the structure of the quadruplets in a non-negligible way (but only in a minor way those of the yellow doublets which are protected from these changes by the red chains). This fact must provide a substantial hindrance for the development of this structural modulation which most likely will be of small amplitude and thus difficult to detect except on transport measurements, as found in the experimental studies.

Note that the only aspect of the electronic structure that may depend on the details of the computational method used is the existence/absence of the closed pockets around Z. The occurrence of these pockets may subtly depend on slight structural differences (compare for instance Figs. 2a and S2 on SI obtained with the same functional and slightly different

geometries showing a small variation of the pocket size) or even on the functional. This is a well known fact on which we commented before for $NbSe_3$.[8,9] The same ambiguity also occurs on the experimental side (see the experimental results for $NbSe_3$ quoted in refs.[7,8] which have been attributed to an electron doping of some samples due to a slight non-stoichiometry). In the present case, closed pockets around Z for strictly stoichiometric samples should occur according to the PBE functional although their real size may depend upon fine structural details. However, this ambiguity is not relevant in the present context since because the nesting of the Fermi surfaces is not perfect, other small closed pockets will occur at low temperature after the three CDWs develop. Additional calculations show that the disappearance of the pockets does not affect in any significant way the response function (i.e. only a minute change on the b^* component of the nesting vector of the order of the precision of the calculations).

In short, we propose that the two q_0 and q_1 high temperature transitions affect the chains of the quadruplet and doublet, respectively. Because of the different nature of these fragments there is a charge transfer from the doublet to the quadruplet which results with CDWs with different b^* components. These two b^* wave vector components practically add to the commensurate value 2/3. Consequently, the third and still non structurally characterized CDW modulation, which will destroy most of the remaining carriers of the quadruplets, should have a nearly commensurate component of 1/3 along the chain.

"$NbSe_3$"-type polymorph: changing the filling of the Nb d_{z^2} bands

Kikkawa and coworkers[26] reported the preparation of a high pressure form of NbS_3, NbS_3-HP, with cell constants (monoclinic $P2_1/m$, a= 9.68 Å, b= 3.37 Å, c= 14.83 Å, β=109.9°) very similar to those of $NbSe_3$ (monoclinic $P2_1/m$, a= 10.009 Å, b= 3.4855 Å, c= 15.641 Å, β=109.49°[11]). However, their sintered powder pellets exhibited a semiconducting behaviour similar to that of NbS_3-I in contrast with the metallic character found for $NbSe_3$. In another work[28] NbS_3 crystals obtained after annealing nearly stoichiometric samples were

considered to correspond to sulfur-rich NbS_3 with compositions between $NbS_{3.5}$ and NbS_4. These crystals although having a semiconducting behavior and apparently the same crystal structure as NbS_3-I, exhibited two resistivity anomalies as for $NbSe_3$[11,13] and isostructural m-TaS_3.[16] Indeed these transitions occur at temperatures around 235 K and 140 K[28] which are extremely similar to those of m-TaS_3, 235 K and 160 K.[16] Unfortunately, for all of these NbS_3 samples, only very limited structural information could be obtained: the space group and lattice parameters for the high pressure samples and some indications about the periodicity along the chains (b cell parameter) for the sulfur rich samples, so that it has not been possible to clarify their structure and transport properties.

One of the seven polymorphs that we have located is isostructural with $NbSe_3$ and m-TaS_3 (see the "$NbSe_3$"-type polymorph in Table 1). The lattice parameters of this optimized structure are very close to those reported by Kikkawa and coworkers[26] and the optimized structure (Table S-I in SI) exhibits all structural details characterizing the $NbSe_3$ and m-TaS_3 crystal structures (see Fig. 1a): (i) three different types of trigonal prismatic chains, (ii) a doublet of *tilted* chains (type III chains), (iii) two chains with one of the triangular S-S sides compatible with a S-S bond (chain I: 2.151 Å, chain III: 2.101 Å) and one chain where it is not (chain II: 2.705 Å). As shown in Table 1 the relative stability of this polymorph with respect to NbS_3-I is computed to be practically the same as that of NbS_3-II, so that we can deduce that it is very likely that this polymorph may actually exist and it is possible that the NbS_3-HP phase is actually this "$NbSe_3$"-type polymorph.

The calculated band structure around the Fermi level for this polymorph is shown in Fig. 4a. In this figure the size of the green, red and blue circles is proportional to the Nb_I, Nb_{II} and Nb_{III} character of the corresponding bands. We use the labelling shown in Fig. 1a for the chains, which also parallels that used for NbS_3-II, i.e. the tilted doublet is made of type III chains, the chains with the long S...S triangular side are type II chains and the doublet of chains corresponding to the quadruplet in NbS_3-II is made of type I chains. As it was the case for the NbS_3-II polymorph, the bands based on the $Nb_{II}S_3$ chains lie above the

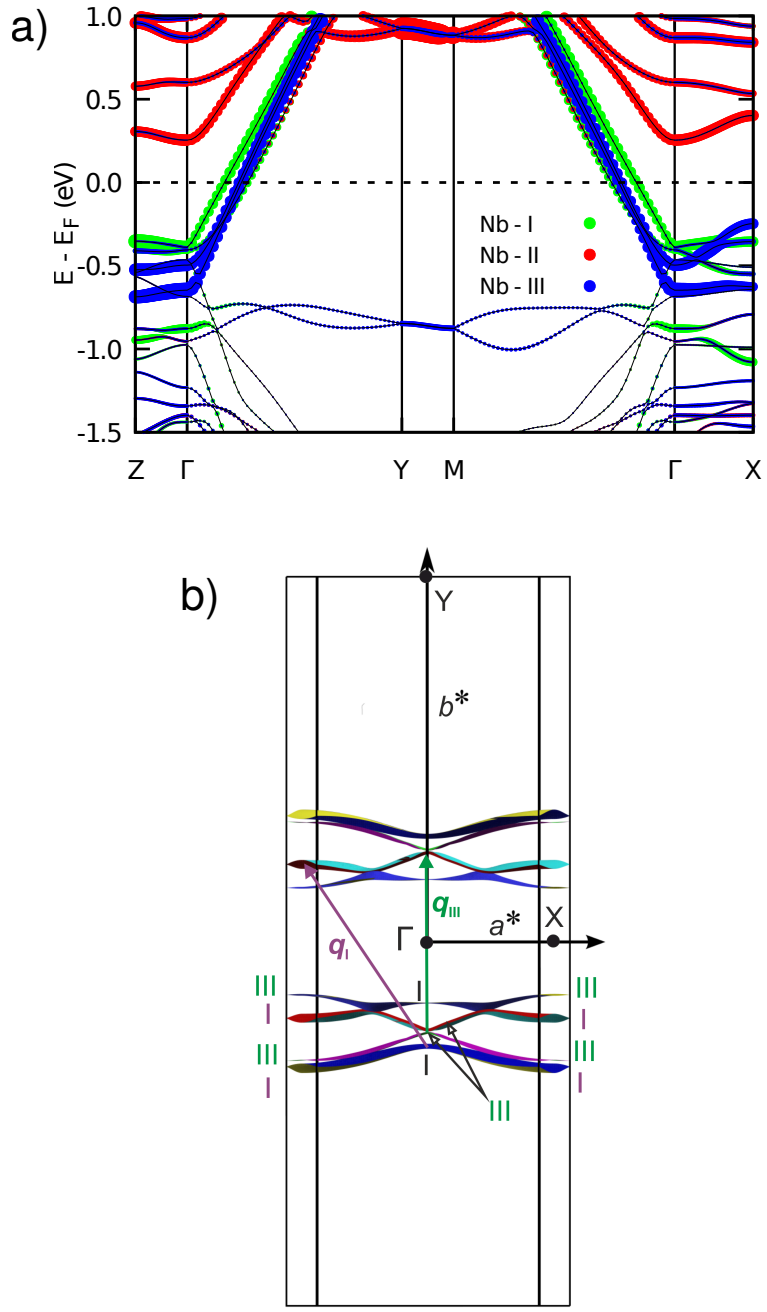

Figure 4: (a) Band structure for "$NbSe_3$"-type NbS_3 calculated using the optimized crystal structure and the PBE functional. Γ= (0, 0, 0), X= (1/2, 0, 0), Y= (0, 1/2, 0), M= (0, 1/2, 1/2) and Z=(0, 0, 1/2) in units of the monoclinic reciprocal lattice vectors. The size of the blue, red and green dots are proportional to the Nb_I, Nb_{II} and Nb_{III} character, respectively (see Fig. 1). (b) Calculated Fermi surface. The different colors are only a help to the view and are unrelated to the chain type character of the different FS sheets. The chain I or chain III character of the FS sheets is shown. Two nesting vectors relevant for the discussion are shown.

Fermi level and thus should not be primarily affected by the onset of the CDW modulations. The $Nb_{III}S_3$ and Nb_IS_3 chains lead to the two inner (blue) and outer (green) partially filled bands, respectively. According to the stoichiometry and the same electron counting scheme used above, the average filling of these four bands is 1/4, instead of 1/3 in NbS_3-II, and the polymorph should exhibit metallic properties. In all respects the main features of this band structure are very similar to those of NbS_3-II except for a slightly weaker interaction between the tilted chain III doublets and those of the non-tilted chain I. Note that, as it happens for m-TaS_3,[9] the type II chain bands do not cross the Fermi level so that no closed pockets seem to occur in the MS_3 (M= Nb, Ta) monoclinic phases with this structure.

The calculated Fermi surface is shown in Fig. 4b where the chain character on which the four different FS sheets are based is also given. Note the very weakly avoided crossing between the two inner pairs of sheets. The larger warping of the sheets based on the tilted type III chains is due to the short inter-layer S...S contacts. Not surprisingly, the analysis of the Fermi surface and Lindhard response function goes along the same lines as in our previous work for m-TaS_3[9] to which we refer for further details. We find two nesting vectors q_{III}=(0a*, 0.247b*, 0c*) and q_I= (0.5a*, 0.250-0.251b*, 0.5c*) (see Fig. 4b) associated with structural modulations affecting type I and type III chains, respectively, which would destroy the four sheets of the FS. Thus, we predict the occurrence of two resistivity anomalies for this polymorph, as it is the case for m-TaS_3[16] and $NbSe_3$.[11,13] Based on the absence of closed pockets and the kind of warping of the FS sheets, this polymorph should most likely exhibit a semiconducting behavior after the two CDW transitions.

We remind that (i) the lattice parameters of the samples prepared by Kikkawa and coworkers[26] are very similar to the ones we obtain (see Table 1), and (ii) the so-called sulfur rich crystals of NbS_3 obtained after annealing nearly stoichiometric crystals,[28] even if being semiconducting, exhibited two resistivity anomalies at 235 K and 140 K. These transition temperatures are very similar to those of the m-TaS_3 which, as mentioned above, exhibits a FS extremely similar to that computed for "$NbSe_3$"-type NbS_3. Thus we believe that the

so-called sulfur rich NbS_3 phase may contain a mixture of both polymorphs, semiconducting NbS_3-I *and* "$NbSe_3$"-type NbS_3. In addition, we suggest that the high pressure NbS_3 prepared by Kikkawa and coworkers[26] is most likely to actually be the "$NbSe_3$"-type polymorph. The reason for the observed semiconducting behavior for the sintered powder pellets is probably due to a transformation from the "$NbSe_3$"-type polymorph to the more stable semiconducting NbS_3-I one occurring during the sintering process. Taking into account all these considerations, we suggest that it may be worthwhile to revisit the high pressure synthesis of NbS_3.

The NbS_3-II and "$NbSe_3$"-type polymorphs are just two members of a family of MX_3 (M= Nb, Ta; X= S, Se) layered solids containing both a tilted doublet and an n-plet (n= 2, 4,...) of regular chains (i.e. containing a short X-X distance), connected by two separated chains without any short S-S contact. These phases will contain n+2 partially dispersive bands and have a total of n electrons to fill them so that the average occupation will be $n/(2n+4)$ and could thus exhibit one CDW associated with the tilted doublets and several (from 1 to $n/2$) CDWs associated with the n-plets.

A polymorph with the same number of isosceles and equilateral-type chains

$TaSe_3$ is the only known group V transition metal trichalcogenide exhibiting the layered crystal structure of Fig. 1c which contains only two different types of chains. The different ratio between chains with a broken (equilateral-like, type II) and unbroken (isosceles-like, type I) X-X short triangular side with respect to the previously examined polymorphs changes the formal average d electron count and, consequently, the filling of the lower transition metal based bands, a feature that drastically influences the transport properties. In contrast with the metallic members of this series, $TaSe_3$, which is really a semimetal, does not exhibit CDW instabilities and keeps the metallic conductivity until very low temperatures, entering into a superconductiong state at around 2 K .[47–49] However, the occurrence of a CDW state has

been claimed to occur in $TaSe_3$ mesowires at 65 K .[50] A high breakdown current density[36,51] and low-frequency electronic noise[35] in microwires have been recently reported for $TaSe_3$, suggesting potential applications in downscaled electronics. It has also been proposed that bulk $TaSe_3$ may be an appropriate system where to study the competition between superconducting and topological phases.[52,53] Recently, single-layer $TaSe_3$ nanoribbons on SiO_2/Si substrates have been obtained through a mechanical exfoliation procedure[37] and a theoretical study[32] has proposed that an interesting competition between metallic and semiconducting states can occur under the effect of strain.

"$TaSe_3$"-type polymorph

As shown in Table 1, the relative stability of the "$TaSe_3$"-type structure of NbS_3 (optimized structure in Table S-II of SI) with respect to NbS_3-I is computed to be in between those of NbS_3-II and NbS_3-V, both of which are known. Thus we believe that such polymorph may also be actually prepared. The calculated band structure is shown in Fig. 5a. The system is found to be semimetallic leading to the Fermi surface of Fig. 5d containing hole (Fig. 5b) and electron (Fig. 5c) portions. The latter originates in a major way from Nb d_{z^2} states of the regular chains I (see Fig. 1c). The holes originate predominantly from S $3p_z$ states of the sulfur atoms of the open type II chains interacting directly with the Nb atoms of the regular type I chains (i.e. the S atoms marked with an asterisk in Fig. 1c). Note that the two bands undergo a real crossing along the Γ-Z line suggesting the possibility of topological effects as discussed for $TaSe_3$ itself.[52,53] Let us note that the semimetallic overlap is kept after inclusion of spin-orbit coupling effects.

In fact, the electronic structure is even more interesting because of the occurrence of a third band which is filled, but almost touches the Fermi level inside the BZ (see for instance the Γ-Y line in Fig. 5a. As we examined in detail elsewhere[32] for the related case of $TaSe_3$ single-layers, the bump of this band is very sensitive to strain along the $(a+c)$ intra-layer direction. Under a small strain along such direction the bump can cross the Fermi level

leading to pairs of additional pockets. Because of these two features, possible topological effects and strain induced FS variations, both of which depend on subtle structural details, this polymorph could exhibit very challenging properties.

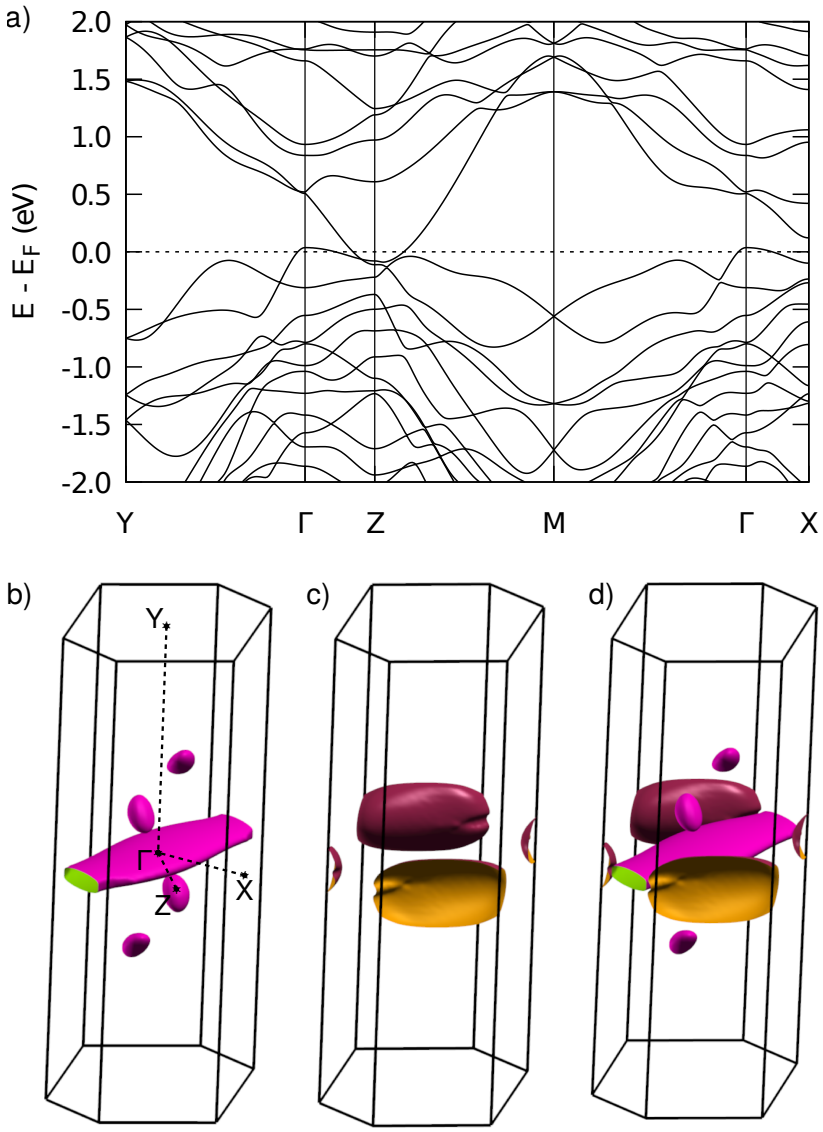

Figure 5: (a) Band structure for "$TaSe_3$"-type NbS_3 calculated using the optimized crystal structure and the PBE functional. Γ= (0, 0, 0), X= (1/2, 0, 0), Y= (0, 1/2, 0), M= (0, 1/2, 1/2) and Z=(0, 0, 1/2) in units of the monoclinic reciprocal lattice vectors. (b-d) Calculated Fermi surface: (c) Holes contribution, (d) Electrons contribution, (d) Full Fermi surface.

Finally, let us note that as for most semimetallic systems, the existence of a band overlap or a band gap may be a delicate question. Our PBE results are consistent with recent GGA-type DFT calculations for $TaSe_3$, either all-electron plane-wave based[52] and local orbital-

based with pseudopotentials.[32] Most details of the band structure are very similar and the semimetallic overlap is a bit smaller in NbS_3 as it should be expected for a sulfur-based compound. We thus believe that the calculated electronic structure of this polymorph is accurate enough.

A possible new family of MX_3 polymorphs

NbS_3 with this structure can be considered as a member of the family of the previously discussed polymorphs with n=1 and no tilted chain doublet. Breaking (i.e. reducing) one S-S bond in the isosceles triangles creates inter-chain tension and leads to a rearrangement ending with a tilted chain doublet. However, the reasons behind such rearrangement are more subtle than just avoiding unwanted S...S repulsions. In the parent TiS_3 structure (Fig. 1b) all the S^{2-} atoms are stabilized by making Nb-S bonds with neighboring chains (i.e. the capping Nb-S bonds). The rearrangement leading to the tilted doublet does not only relieve the S...S inter-chain interactions *but* facilitates also that one of the two created S^{2-} can be stabilized by forming one of these capping Nb-S bonds with the Nb atom of one of the tilted chains. What the structure of $TaSe_3$ is telling us is that there is a second way to reach the same kind of stabilization without creating tilted chains just by pairing these open chains in a doublet. A layer of $TaSe_3$ can be seen as a succession of doublets of open and regular chains (but note that the two types of doublets are slightly different). This simple structural view immediately opens the possibility for the existence of another family of MX_3 polymorphs in which one such double unit of open chains separates n-plets of regular chains. For the time being $TaSe_3$ seems to be the lower (n= 2) and only known member of this family. The values reported in Table 1 suggest that the "$TaSe_3$"-type NbS_3 polymorph may be stable even if generation of a tilted doublet of regular chains seems to be somewhat more favorable than the creation of a doublet of open chains. It is also tempting to propose that a new family of MX_3 polymorphs may actually exist. Although the "$TaSe_3$"-type polymorph is predicted to be a semimetal, the higher members of this new series (n= 4, 6,...) will possess

n partially dispersive bands and have a total of n-2 electrons to fill them so that the average band occupation will thus be (n-2)/2n= 0.5-(1/n). These phases should thus be metallic and could exhibit several (from 1 to n for n= 4, 6....) CDWs associated with the n-plets.

Metallic (NbS_3-V and NbS_3-V') vs. semiconducting (NbS_3-I) polymorphs: A non-conventional Peierls distortion?

For several decades NbS_3-I was the only structurally well characterized NbS_3 polymorph[20] but recently Balandin, Salguero and coworkers[27] reported the crystal structure of two new polymorphs, NbS_3-IV and NbS_3-V. The latter is very interesting since it exhibits the same structure as NbS_3-I, with the same layer packing (ABCDE, see Fig. S5 in SI), *but* without Nb-Nb pairing, i.e. with half the periodicity along the chains direction. This is the structure of TiS_3 (Fig. 1b) which is formally seen as the structure of NbS_3 before the Peierls distortion. Thus, NbS_3 is one of the rare compounds which can be prepared with the structure both before and after the Peierls distortion. The transport properties of this polymorph were not reported although it should exhibit metallic behavior.

Polymorphs with a non-dimerized TiS_3-type structure

Non-dimerized structures were indeed considered in our search and, as shown in Table 1, two different polymorphs of this type were located. One of them is the NbS_3-V polymorph reported by Balandin, Salguero and coworkers.[27] The optimized structure is in excellent agreement with the reported crystal structure (Table 1). To our surprise we located a second polymorph which is even a bit more stable. This polymorph is similar to NbS_3-V in the sense that it is non-dimerized along the chains direction, the unit cell contains a single layer and the layers pack in an ABCDE mode (Fig. S5 in SI). Thus, we designate this polymorph as NbS_3-V'. However, an important difference between the two polymorphs occurs in the sulfur sublattice. Whereas for NbS_3-V, as for NbS_3-I (and NbS_3-IV to be discussed in the next section), there is a large difference between the intra-chain S-S bond and the inter-chain

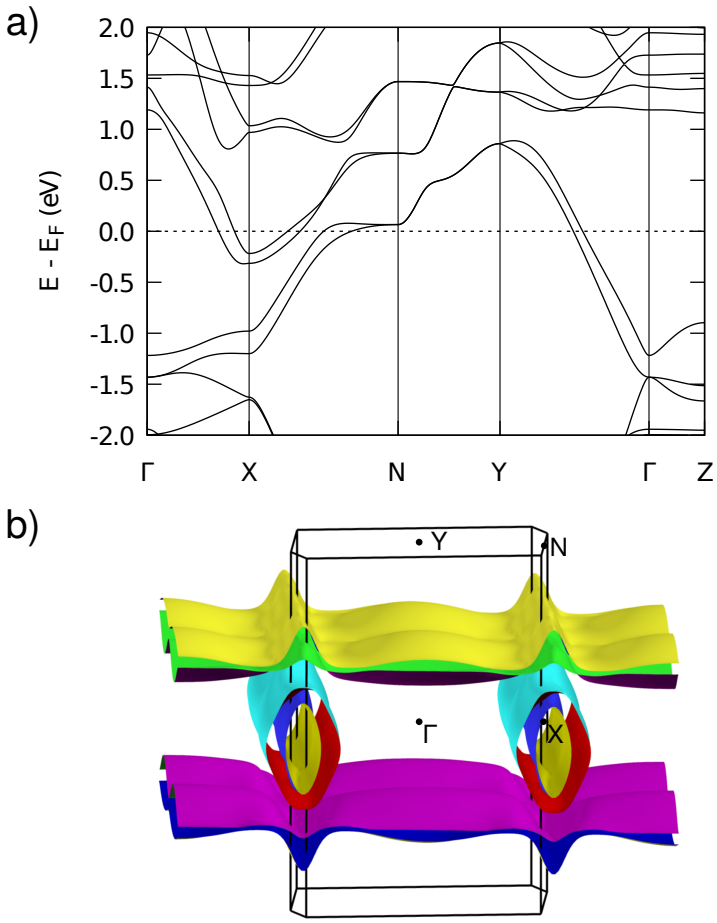

Figure 6: (a) Band structure for NbS_3-V calculated using the experimental crystal structure and the PBE functional. Γ= (0, 0, 0), X= (1/2, 0, 0), Y= (0, 1/2, 0), N= (1/2, 1/2, 0) and Z=(0, 0, 1/2) in units of the monoclinic reciprocal lattice vectors. (b) Calculated Fermi surface.

S...S contact along the a-direction (i.e. **b** and **nb** in Fig. 1b), 2.019 Å vs. 2.931 Å or 2.050 Å vs. 2.913 Å in the experimental structures of NbS_3-V and NbS_3-I respectively, they are considerably more similar, 2.227 Å vs. 2.551 Å in the optimized structure of NbS_3-V' (Table S-III in SI). This is not an artifact of the computational approach since our calculations perfectly reproduce the mentioned strong difference occurring in the experimental structure of NbS_3-I and NbS_3-V (calculated values: 2.035 Å vs. 2.937 Å for NbS_3-I and 2.055 Å vs. 2.890 Å for NbS_3-V). Indeed this kind of "long" bonds and "short" non-bonded contacts occur in other of the structures discussed. For instance in the crystal structure of NbS_3-II, there are S-S bonds of 2.040, 2.186 and 2.208 Å as well as non-bonded contacts of 3.012, 2.752 and 2.582 Å. A similar situation can be found in selenides like $NbSe_3$ and $TaSe_3$, clearly witnessing the versatility of the chalcogen sublattice in these compounds which is one of the main reasons for the rich polymorphism.

An unusual Peierls distortion: interchain interactions

The calculated band structure for NbS_3-V is shown in Fig. 6a. According to the well accepted view of the dimerized structure of NbS_3-I as the result of a Peierls distortion, we should expect a simple band structure with a half-filled and dispersive Nb d_{z^2}-based band. However, this is not what can be seen in Fig. 6a. Indeed the simple description could be taken as grossly correct if we just look at the Γ-Y direction in Fig. 6a (i.e. the chains' direction) where a pair of dispersive and not far from half-filled Nb d_{z^2} bands associated with the two non-dimerized chains of the unit cell can be seen. However, if we look at other directions of the BZ (for instance X-N) we can see that a second pair of bands that undergoes an avoided crossing with these Nb d_{z^2} bands precisely around the Fermi level. This second pair of bands has a strong dispersion along the X-Γ direction (i.e. the inter-chain a^*-direction) and consequently introduces substantial intra-layer inter-chain interactions into the states around the Fermi level. This can be clearly seen in the calculated FS of Fig. 6b. It results from the hybridization of two pairs of planes perpendicular to the direction of the chains

(Γ-Y) and two closed cylinders with ellipsoidal section approximately along the inter-layer c^*-direction and centered at the X point.

The simple description of the Peierls distortion would require the absence of the two cylinders. Indeed, whatever structure is used for the calculations, the experimental or the HSE06 optimized one (see the calculated band structure with the HSE06 optimized geometry in Fig. S6 of SI), these cylinders always occur in the FS. Thus, although nesting is obviously present in the FS, because of the occurrence of the cylinders the nesting vector can not have the commensurate $0.5b^*$ component required for a dimerization but an incommensurate value. In addition, even if such incommensurate structural modulation could occur, the polymorph would keep the metallic properties because of the existence of the cylinders, as well as the additional pockets created by the modulation due to the corrugation (imperfect nesting) of the FS sheets. This new scenario with an incommensurate CDW modulation not far from dimerization is completely new within the MX_3 (M= Nb, Ta, X= S, Se) low-dimensional solids and thus it would be very interesting to study the transport properties of this new NbS_3-V polymorph in detail. It is worth pointing out that a theoretical study of the injection of carriers through electric field gating in single-layers of TiS_3, where electrons are injected into the same type of band that we are discussing, indeed predicted the possibility of CDW-type anomalies.[54] Later experimental work reported transport measurements suggesting CDW formation although a more complete characterization is still needed.[55–58]

The previous discussion makes clear that the origin of the pairing in NbS_3-I is not as simple as it is commonly believed. The reason is the existence of a second pair of bands undergoing an avoided crossing with the "expected" Nb d_{z^2} bands. This pair of bands originates from the Nb d_{xy} orbitals which are raised in energy because of the Nb-S capping interaction. These orbitals lead to a strongly dispersive band going down along the Γ-X direction, i.e. the intra-layer inter-chain direction. Consequently, the avoided crossing introduces inter-chain interactions into the Nb d_{z^2} bands. The main character of the Nb d_{xy}-based band at the Γ point is sketched in Fig. 7. Around Γ all capping Nb-S interactions

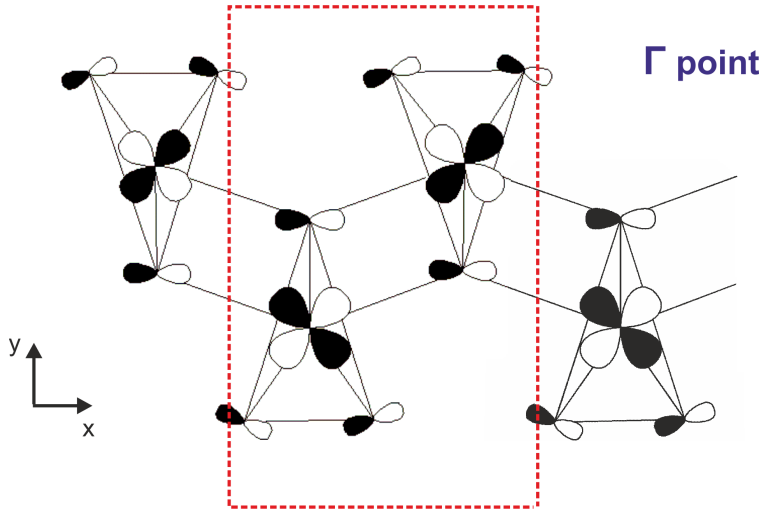

Figure 7: Nature of the band introducing inter-chain coupling into the Nb d_{z^2} pair of bands (Γ point).

are antibonding. However at the X point the sign of the crystal orbital changes on adjacent cells so that half of the Nb-S interactions become bonding (and half remain antibonding) so that the crystal orbital becomes globally Nb-$S_{capping}$ non-bonding and hence, when going from Γ to X the band is strongly lowered in energy as seen in Fig. 6a. Note that this band contains substantial S p_x character which, around the X point, is antibonding within the S-S bond but bonding in between S-S bonds. When going down along the Γ to X direction this S-S contribution is considerably enhanced providing an additional source of stabilization of the band around X. In other words, although in large parts of the BZ the half-filled band of NbS_3-V is dominated by the Nb d_{z^2} orbitals, the planes near the border of the BZ along the a^*-direction introduce substantial inter-chain interactions and, hence, the classical description of the origin of the dimerized structure of NbS_3-I is not really correct (see further discussion in the next section).

As noted above, the band introducing inter-chain interactions around the border of the BZ contains very substantial S p_x character which around the X point is antibonding within the S-S bond but bonding in-between S-S bonds. Consequently, changing the S-S distances within and between chains (**b** and **nb** in Fig. 1b) as it actually happens in the NbS_3-V' polymorph will disturb the role of the inter-chain interactions in the band structure (Fig. S7

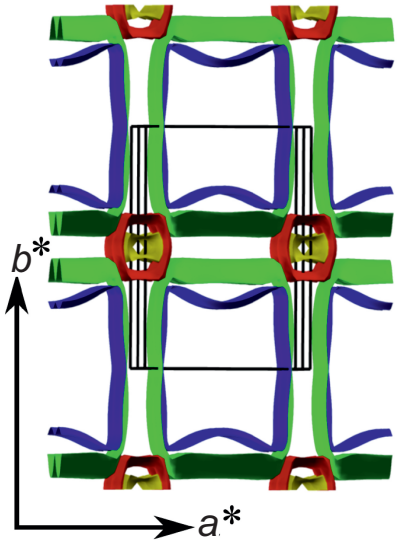

Figure 8: Calculated Fermi surface for the NbS_3-V' polymorph.

in SI) and the shape of the FS can be somewhat altered. The calculated FS for the NbS_3-V' polymorph is shown in Fig. 8. Because of a small shift in the pair of bands introducing inter-chain interactions, the FS now contains flat portions along both directions of the layer and different instabilities can be expected. Clearly, these "TiS_3"-type polymorphs can provide ground for a very interesting physics.

Dimerized polymorphs (NbS_3-I and NbS_3-IV)

The well known NbS_3-I polymorph[20] can be considered as the upper member of the NbS_3-II family with n very large and thus no partially filled bands. It is found to be a semiconductor with a strong Nb-Nb dimerization along the chains (3.037 Å and 3.693 Å). More recently, Balandin, Salguero and coworkers[27] reported another polymorph, NbS_3-IV, with a very similar dimerization (3.045 Å and 3.709 Å) which exhibits somewhat different inter-layer interactions but very similar volume per formula unit (see Table 1). The inter-layer stacking is of the ABCDE-type in NbS_3-I but AB in NbS_3-IV (see Fig. S5 in SI). Our optimized structures are in excellent agreement with the crystal structures (for instance Nb-Nb distances of 3.028

Å and 3.719 Å for NbS_3-I). Both polymorphs are practically equally stable (Table 1) so that it can not be excluded that inter-layer stacking disorder can occur in some samples.

As shown in Fig. 6, for a relatively large part of the BZ the classical description of the "TiS_3"-type structure of NbS_3, with a pair of half-filled Nb d_{z^2} -type bands leading to planar sheets in the FS separated by $\sim 1/2b^*$, indeed holds. However, as we approach the border of the BZ along the a^* direction (i.e. the intra-layer inter-chain direction) this picture is strongly perturbed because of the inter-chain interactions occurring for wave vectors in that part of the BZ. Thus, in order for the commensurate dimerization to occur there must be some additional distortion that removes this inter-chain couplings from the FS (most likely some breathing of the S-Nb-S capping angle which will destabilize the Nb d_{xy}-based antibonding band). Only then, the classical picture of well-nested half-filled Nb d_{z^2} bands holds and the dimerization may occur. In that sense, the Peierls distortion of these semiconducting NbS_3 polymorphs should be better qualified as a "Peierls-assisted" distortion.

The band structures calculated with the HSE06 hybrid functional for the NbS_3-I and NbS_3-IV phases are reported in Figs. 9 and S8a of SI, respectively. Both polymorphs are indirect band gap semiconductors with energy gaps of 0.91 (NbS_3-I) and 1.06 eV (NbS_3-IV). As usual for semiconductors, the calculated HSE06 band gaps are in excellent agreement with experimental values (0.83 - 1.1 eV for NbS_3-I[2,59]). Let us note that the calculated band gap with the PBE functional[21] is smaller than the HSE06 one but the calculated band structure is practically the same except for a nearly rigid shift of the conduction band (see for instance Figs. S8a and b on SI for the band structure of NbS_3-IV polymorph with the two functionals). The nature of the states at the top of the valence band and bottom of the conduction band is based on the Nb-Nb antibonding combination of the Nb d_{z^2} orbitals (somewhat hybridized with the Nb s and p_z orbitals so as to accumulate a bit more of electron density along the long Nb-Nb distance) and the p_x and p_y orbitals of the capping S atoms, respectively. Note that the crystal structures of the NbS_3-I and NbS_3-IV polymorphs are given with different systems of axes: the chain axis is b in NbS_3-I but a in NbS_3-IV. Although

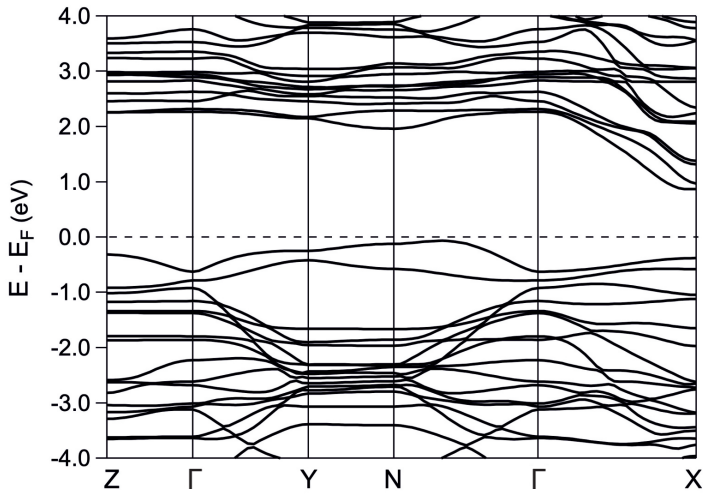

Figure 9: Band structure for NbS_3-I calculated using the experimental crystal structure and the HSE06 functional. Γ= (0, 0, 0), X= (1/2, 0, 0), Y= (0, 1/2, 0), N= (1/2, 1/2, 0) and Z=(0, 0, 1/2) in units of the monoclinic reciprocal lattice vectors. The energy zero is the highest occupied energy level.

the two band structures of Figs. 9 and S8a on SI could seem to be different, they are really almost identical when the different axes, as well as the doubling of the bands for NbS_3-IV is taken into account. Consequently, no significant differences in their properties are expected for the two polymorphs (except for some phonon-related ones). As noted above, NbS_3-I, which is the more stable polymorph, has also the larger unit cell. However, the stability of this polymorph (as well as that of NbS_3-IV) is an electronic effect due to the opening of a band gap at the Fermi level and not a volumetric effect, as shown by the fact that here is no clear relationship between stability and size of the unit cell when the seven polymorphs are considered (see Table 1).

Concluding remarks

When extra electrons are introduced into the very stable layered TiS_3-type structure by using a group V transition metal atom either (i) metal-metal bonding (i.e. commensurate or incommensurate CDW or Peierls distortions) or (ii) S-S bond reduction (i.e. formation of equilateral trigonal prismatic chains) can occur. The ratio between the number of electrons used in the two processes will impose the shape of the trigonal prismatic based layers and subtly change the d^x $(0 < x < 1)$ electron count of the transition metal atoms and consequently, the electronic structure and properties of the solid. This is suggestive that some group V trichalcogenides should be prone to occur in several polymorphic forms with different properties and that the presently known systems may well be just the tip of the iceberg.

Based on both already existing experimental and new theoretical results we have considered this aspect for NbS_3 and found that *at least* seven different polymorphs are possible. One is the well known NbS_3-I, three correspond to the recently characterized NbS_3-II, NbS_3-IV and NbS_3-V phases and the other remaining three are so-far non-reported polymorphs with the structures of $NbSe_3$, TiS_3 and $TaSe_3$, respectively. From the energetic point of view,

the stability of these new polymorphs is compatible with those of the presently known ones. We have shown that this series of low-dimensional polymorphs should display a rich variety of physical behaviors (Fig. 10). The well-known view of the dimerized structure of the semiconducting NbS_3-I polymorph as a typical example of a Peierls distortion is discussed and shown to be only partially correct because inter-chain interactions are stronger than naively expected. The NbS_3-V, NbS_3-II and "$NbSe_3$"-type polymorphs are (or are predicted to be) metallic systems with incommensurate CDW instabilities associated with half-, third- and quarter-filling of the Nb d_{z^2} bands of the trigonal prismatic chains, respectively. This series of polymorphs thus provides a clear-cut illustration of the intimate link between structural and electronic features for a structurally related family of materials. Note that we have not considered an exhaustive list of possible polymorphs. Other can be conceived. For instance, we have pointed out a particularly appealing family based on the $TaSe_3$ structure. Our purpose here is to emphasize that the combined use of structural and electronic ideas can provide very useful hints in the search for these polymorphs.

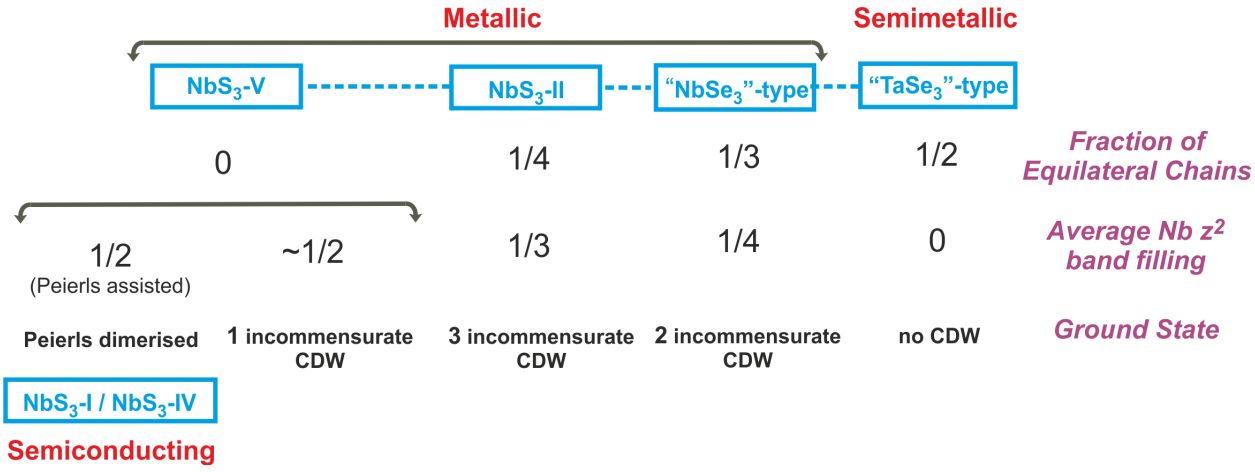

Figure 10: Summary of the different NbS_3 polymorphs discussed in this work (The NbS_3-V' is a variety of NbS_3-V slightly differing in the sulfur sublattice).

It is worth noticing that several of the phases discussed here (and even their contrasting properties) may have been prepared in the past although in an uncontrolled way that prevented their full characterization. A careful look at Table I in the work by Izumi *et al.*[28]

with the present results in mind, suggests that depending on the preparation conditions (temperature, sulfur pressure, annealing, etc.) at least four different products were found: (i) the semiconducting NbS_3-I polymorph, (ii) a mixture of semiconducting NbS_3-I and a metallic phase most likely the "$NbSe_3$" type polymorph, (iii) a mixture of semiconducting NbS_3-I and a metallic (and superconducting) phase most likely the NbS_3-V and/or NbS_3-V' type polymorphs, and (iv) a metallic and superconducting phase most likely the NbS_3-V and/or NbS_3-V' type polymorphs. T_c of the superconducting phase is very similar to that of the $NbSe_3$ (or *m*-TaS_3) under pressure when the CDW is suppressed.[4] This observation thus strongly suggests that a chemical control of the phase diagram can most likely be attained. Also, in view of these comments we urge investigation of the transport properties of the already prepared NbS_3-V phase and point out the importance of single crystal structural determinations in unambiguously distinguishing the different polymorphs..

The very rich landscape of different structures and properties of these low-dimensional polymorphs should provide a strong stimulus for studying these materials as flakes with different number of layers as a basis for the development of new electronic and optoelectronic devices. Chemical doping by preparation of Nb/TiS_3 alloys has been recently reported[60–62] thus bringing additional expectations for the very rich diversity of physical and chemical behaviour of NbS_3 (and probably also the other M/X; M= Nb, Ta, X= S, Se) polymorphs.

Experimental Section

All calculations were carried out using first-principles density functional theory (DFT).[63,64] The structural optimizations and evaluation of the relative energies of the different polymorphs were carried out using the *ab initio* CRYSTAL17 code.[65–67] All other calculations were carried out using a numerical atomic orbitals density functional theory (DFT) approach implemented in the SIESTA code.[68–70] Full details about the computations are reported in the Supporting Information.

Supporting Information

Details of the DFT calculations. (Figure S1) Labeling of the special points of the monoclinic Brillouin zone used in this work. (Figure S2) Band structure of NbS_3-II calculated using the HSE06 optimized structure and the PBE functional. (Figure S3) Fatband analysis of the band structure of NbS_3-II calculated using the experimental structure and the PBE functional. (Figure S4) A rotated view of the Fermi surface of NbS_3-II. (Figure S5) Comparison of the different stackings of the NbS_3 bilayers in polymorphs Nb_3-I and Nb_3-IV. (Figure S6) Band structure for NbS_3-V calculated using the HSE06 optimized structure and the PBE functional. (Figure S7) Band structure for NbS_3-V' calculated using the HSE06 optimized structure and the PBE functional. (Figure S8) Band structure of NbS_3-IV calculated using the experimental crystal structure and (a) the HSE06 and (b) PBE functionals. (Table S-I) Calculated crystal structure for the NbS_3 polymorph with the "$NbSe_3$"-type structure using the HSE06 hybrid functional; (Table S-II) Calculated crystal structure for the NbS_3 polymorph with the "$TaSe_3$"-type structure using the HSE06 hybrid functional; (Table S-III) Calculated crystal structure for the NbS_3-V' polymorph using the HSE06 hybrid functional.

Author Information

Authors

Sergio Conejeros- E-mail: sconejeros@ucn.cl; ORCID: 0000-0002-2490-1677

Bogdan Guster- E-mail: bogdan.guster@gmail.com; ORCID: 0000-0003-1305-1862

Pere Alemany- E-mail: p.alemany@ub.esdu; ORCID: 0000-0002-3139-6189

Jean-Paul Pouget- E-mail: jean-paul.pouget@u-psud.fr; ORCID: 0000-0002-6244-389X

Enric Canadell- E-mail: canadell@icmab.es; ORCID: 0000-0002-4663-5226

Notes

The authors declare no competing financial interest.

Acknowledgement

This work was supported by the Spanish MICIU through grants PGC2018-096955-B-C44 and PGC2018-093863-B-C22, the Severo Ochoa FUNFUTURE (CEX2019-000917-S) Excellence Centre distinction, the Maria de Maeztu Units of Excellence Program (MDM-2017-0767), and Generalitat de Catalunya (Grants No. 2017SGR1506 and 2017SGR1289). S.C. was supported by FONDECYT, Chile (Project 11171063).

References

(1) Meerschaut, A.; Rouxel, J. In *Crystal Chemistry and Properties of Materials with Quasi-One-Dimensional Structures*; Rouxel, J., Ed.; D. Reidel Publishing Company, Dordrecht, Holland, 1986; pp 205–279.

(2) Island, J. O.; Molina-Mendoza, A. J.; Barawi, M.; Biele, R.; Flores, E.; Clamagirand, J. M.; Ares, J. R.; Sánchez, C.; van der Zant, H. S. J.; D'Agosta, R.; Ferrer, I. J.; Castellanos-Gomez, A. Electronics and optoelectronics of quasi-one dimensional layered transition metal trichalcogenides. *2D Materials* **2017**, *4*, 022003.

(3) Patra, A.; Rout, C. S. Anisotropic quasi-one-dimensional layered transition-metal trichalcogenides: synthesis, properties and applications. *RSC Advances* **2020**, *10*, 36413–36438.

(4) Monceau, P. Electronic crystals: an experimental overview. *Adv. Phys.* **2012**, *61*, 325–581.

(5) Rouxel, J.; Schlenker, C. In *Charge Density Waves in Solids*; Gorkov, L. P., Grüner, C., Eds.; Modern Problems in Condensed Matter Sciences; North Holland, 1989; pp 15–83.

(6) Brazovskii, S.; Brun, C.; Wang, Z.-Z.; Monceau, P. Scanning-Tunneling Microscope

Imaging of Single-Electron Solitons in a Material with Incommensurate Charge-Density Waves. *Phys. Rev. Lett.* **2012**, *108*, 096801.

(7) Nicholson, C. W.; Berthod, C.; Puppin, M.; Berger, H.; Wolf, M.; Hoesch, M.; Monney, C. Dimensional Crossover in a Charge Density Wave Material Probed by Angle-Resolved Photoemission Spectroscopy. *Phys. Rev. Lett.* **2017**, *118*, 206401.

(8) Valbuena, M. A.; Chudzinski, P.; Pons, S.; Conejeros, S.; Alemany, P.; Canadell, E.; Berger, H.; Frantzeskakis, E.; Avila, J.; Asensio, M. C.; Giamarchi, T.; Grioni, M. Polarization dependence on nanoARPES reveals emerging one-dimensionality of electrons in $NbSe_3$. *Phys. Rev. B* **2019**, *99*, 075118.

(9) Guster, B.; Pruneda, M.; Ordejón, P.; Canadell, E.; Pouget, J.-P. Electron-hole response function of transition metal trichalcogenides $NbSe_3$ and monoclinic-TaS_3. December 12, 2020, arXiv:2012.06812v2 [cond-mat.mtrl-sci], http://arxiv.org/abs/2012.06812, last accessed June 2021.

(10) Meerschaut, A.; Rouxel, J. Le seleniure $NbSe_3$: Obtention et structure. *J. Less Common Met.* **1975**, *39*, 197–203.

(11) Hodeau, J. L.; Marezio, M.; Roucau, C.; Ayroles, R.; Meerschaut, A.; Rouxel, J.; Monceau, P. Charge-density waves in $NbSe_3$ at 145 K: crystal structures, x-ray and electron diffraction studies. *J. Phys. C.: Solid State Phys.* **1978**, *11*, 4117–4134.

(12) Chaussy, J.; Haen, P.; Lasjaunias, J. C.; Monceau, P.; Waysand, G.; Waintal, A.; Meerschaut, A.; Molinié, P.; Rouxel, J. Phase transitions in $NbSe_3$. *Solid State Comm.* **1976**, *20*, 759–763.

(13) Fleming, R. M.; Moncton, D. E.; McWhan, D. B. X-ray scattering and electric field studies of the sliding mode conductor $NbSe_3$. *Phys. Rev. B* **1978**, *18*, 5560–5563.

(14) Pouget, J.-P.; Moret, R.; Meerschaud, A.; Guemas, L.; Rouxel, J. X-ray observation of 1-d precursor effects in $NbSe_3$ and new diffuse scattering features in $FeNb_3Se_{10}$. *J. Phys. (France) Colloques* **1983**, *44*, C3.1729.

(15) Meerschaut, A.; Guemas, L.; Rouxel, J. Structure and properties of the new phase of the pseudo one-dimensional compound TaS_3. *J. Solid State Chem.* **1981**, *36*, 118–123.

(16) Roucau, C.; Ayroles, R.; Monceau, P.; Guemas, L.; Meerschaut, A.; Rouxel, J. Electron diffraction and resistivity measurements on the one-dimensional orthorhombic and monoclinic structures of TaS_3. Comparison with $NbSe_3$. *Phys. Stat. Sol. (a)* **1980**, *62*, 483–493.

(17) Canadell, E.; Rachidi, I. E.-I.; Pouget, J. P.; Gressier, P.; Meerschaut, A.; Rouxel, J.; Jung, D.; Evain, M.; Whangbo, M.-H. Comparison of the Electronic Structures of Layered Transition-Metal Trichalcogenides $TaSe_3$, TaS_3 and $NbSe_3$. *Inorg. Chem.* **1990**, *29*, 1401–1407.

(18) Furuseth, S.; Brattås, L.; Kjekshus, A. On the crystal structures of TiS_3, ZrS_3, $ZrSe_3$, $ZrTe_3$, HfS_3 and $HfSe_3$. *Acta Chem. Scand. A* **1975**, *29*, 623–631.

(19) Zupanič, E.; van Midden, H. J. P.; van Midden, M.; Šturm, S.; Tchernychova, E.; Pokrovskii, V. Y.; Zybtsev, S. G.; Nasretdinova, V. F.; Zaitsev-Zotov, S. V.; Chen, W. T.; Pai, W. W.; Bennett, J. C.; Prodan, A. Basic and charge density wave modulated structures of NbS_3-II. *Phys. Rev. B* **2018**, *98*, 174113.

(20) Rijnsdorp, J.; Jellinek, F. The crystal structure of niobium trisulfide, NbS_3. *J. Solid State Chem.* **1978**, *25*, 325–328.

(21) Abdel-Hafiez, M.; Thiyagarajan, R.; Majumdar, A.; Ahuja, R.; Luo, W.; Vasiliev, A. N.; Maarouf, A. A.; Zybtsev, S. G.; Pokrovskii, V. Y.; Zaitsev-Zotov, S. V.; Pavlovskiy, V. V.; Wu Pai, W.; Yang, W.; Kulik, L. V. Pressure-induced reentrant

transition in NbS_3 phases: Combined Raman scattering and x-ray diffraction study. *Phys. Rev. B* **2019**, *99*, 235126.

(22) Zybtsev, S. G.; Pokrovskii, V. Y.; Nasretdinova, V. F.; Zaitsev-Zotov, S. V.; Pryadun, V. V.; Kozlyakova, E. S.; Volkova, O. S.; Vasiliev, A. N.; Wu Pai, W.; Starešinić, D. Thermoelectric power and its correlation with conductivity in NbS_3 whiskers. *Phys. Rev. B* **2019**, *99*, 235155.

(23) Wang, W. W.; Monceau, P.; Salva, H.; Roucau, C.; Guemas, L.; Meerschaut, A. Charge-density-wave transport above room temperature in a polytype of NbS_3. *Phys. Rev. B* **1989**, *40*, 11589–11593.

(24) Zybtsev, S. G. et al. NbS_3: A unique quasi-one-dimensional conductor with three charge density wave transitions. *Phys. Rev. B* **2017**, *95*, 035110.

(25) Zettl, A.; Jackson, C.; Janossy, A.; Grüner, G.; Jacobsen, A.; Thompson, A. H. Charge density wave transition and nonlinear conductivity in NbS_3. *Solid State Comm.* **1982**, *43*, 345–347.

(26) Kikkawa, S.; Ogawa, N.; Koizumi, M.; Onuki, Y. High pressure syntheses of TaS_3, NbS_3, $TaSe_3$ and $NbSe_3$ with $NbSe_3$-type crystal structure. *J. Solid State Chem.* **1982**, *41*, 315–322.

(27) Bloodgood, M. A.; Wei, P.; Aylan, E.; Bozhilov, K. N.; Balandin, A. A.; Salguero, T. T. Monoclinic structures of niobium trisulfide. *APL Materials* **2018**, *6*, 026602.

(28) Izumi, M.; Nakayama, T.; Yoshizaki, R.; Uchinokura, K.; Iwazumi, T.; Seino, T.; Matsuura, E. In *Proc. Int. Symp. on Nonlinear Transport and Related Phenomena in Quasi-One Dimensional Inorganic Conductors*; Sambongi, T., Abe, Y., Eds.; Kyoto University, 1983; pp 301–324, http://hdl.handle.net/2433/91158, last accessed June 2021.

(29) Dai, J.; Li, M.; Zeng, X. C. Group IVB transition metal trichalcogenides: a new class of 2D layered materials beyond graphene. *WIREs Computational Molecular Science* **2016**, *6*, 211–222.

(30) Kang, J.; Sahin, H.; Ozaydin, H. D.; Senger, R. T.; Peeters, F. M. TiS_3 nanoribbons: Width-independent band gap and strain-tunable electronic properties. *Physical Review B* **2015**, *92*, 075413.

(31) Silva-Guillén, J. A.; Canadell, E.; Guinea, F.; Roldán, R. Strain tuning of anisotropy in the Optoelectronic Properties of TiS_3. *ACS Photonics* **2018**, *5*, 3231–3237.

(32) Silva-Guillén, J. A.; Canadell, E. Strain control of the competition between metallic and semiconducting states in single-layers of $TaSe_3$. *2D Materials* **2020**, *7*, 025038.

(33) Fedorov, V. E.; Artemkina, S. B.; Grayfer, E. D.; Naumov, N. G.; Mironov, Y. V.; Bulavchenko, A. I.; Zaikovskii, V. I.; Antonova, I. V.; Komonov, A. I.; Medvedev, M. V. Colloidal solutions of niobium trisulfide and niobium triselenide. *J. Mater. Chem. C* **2014**, *5*, 5479–5486.

(34) Mayorga-Martinez, C. C.; Sofer, Z.; Luxa, J.; Huber, S.; Sedmidubský, D.; Brázda, P.; Palatinus, L.; Mikulics, M.; Lazar, P.; Medlí, R.; Pumera, M. TaS_3 Nanofibers: Layered Trichalcogenide for High-Performance Electronic and Sensing Devices. *ACS Nano* **2018**, *12*, 464–473.

(35) Liu, G.; Rumyantsev, S.; Bloodgood, M. A.; Salguero, T. T.; Shur, M.; Balandin, A. A. Low-Frequency Electronic Noise in Quasi-1D $TaSe_3$ van der Waals Nanowires. *Nano Lett.* **2017**, *17*, 377–383.

(36) Empante, T. A.; Martinez, A.; Wurch, M.; Zhu, Y.; Geremew, A. K.; Yamaguchi, K.; Isarraraz, M.; Rumyantsev, S.; Reed, E. J.; Balandin, A. A.; Bartels, L. Low-Resistivity and High Breakdown Current Density of 10 nm Diameter van der Waals $TaSe_3$ Nanowires by Chemical Vapor Deposition. *Nano Lett.* **2019**, *19*, 4355–4361.

(37) Kim, B. J.; Jeong, B. J.; Oh, S.; Chae, S.; Choi, K. H.; Nasir, T.; Lee, S. H.; Lim, H. K.; Choi, I. J.; Hong, M.-K.; Yu, H. K.; Lee, J.-H.; Choi, J.-Y. Thickness-Dependence Electrical Characterization of the One-Dimensional van der Waals $TaSe_3$ Crystal. *Materials* **2019**, *12*, 2462.

(38) Bjerkelund, E.; Fermor, J. H.; Kjekshus, A. On the properties of TaS_3 and $TaSe_3$. *Acta Chem. Scand.* **1966**, *20*, 1836–1842.

(39) Hoffmann, R.; Shaik, S.; Scott, J. D.; Whangbo, M.-H.; Foshee, M. J. High-Temperature Symmetry Breaking in the Electronic Band Structure of the Quasi-One-Dimensional Solid $NbSe_3$. *J. Solid State Chem.* **1980**, *34*, 263–269.

(40) The $|< i,k \mid \exp(iqr) \mid j,k+q >|^2$ matrix elements take into account the spatial overlap of the $\mid i,k >$ and $\mid j,k+q >$ Bloch functions of bands i and j respectively. Since the partially filled bands are primarily built from d_{z^2} orbitals located either on the quadruplet and doublet chains which are spatially separated in the structure and as the d_{z^2} orbitals are directed along the chain direction, the matrix elements associated with the overlap of quadruplet and doublet wave functions should be much smaller than those associated with the overlap of the inner quadruplet or doublet wave functions. Thus the Lindhard function should be primarily the sum of the separate contributions of the quadruplet and doublet.

(41) Pokrovskii, V. Y.; Zybtsev, S. G.; Nikitin, M. V.; Gorlova, I. G.; Nasretdinova, V. F.; Zaitsev-Zotov, S. V. High-frequency, quantum and electromechanical effects in quasi-one-dimensional charge density wave conductors. *Physics-Uspekhi* **2013**, *56*, 29–48.

(42) Zybtsev, S. G.; Pokrovskii, V. Y.; Nasretdinova, V. F.; Zaitsev-Zotov, S. V. Growth, crystal structure and transport properties of quasi one-dimensional conductor NbS_3. *Physica B: Condens. Matt.* **2012**, *407*, 1696–1699.

(43) Boswell, F. W.; Prodan, A. Peierls distortions in NbS_3 and $NbSe_3$. *Physica B* **1980**, *99*, 361.

(44) Zybtsev, S. G.; Pokrovskii, V. Y.; Nasretdinova, V. F.; Zaitsev-Zotov, S. V. Gigahertz-range synchronization at room temperature and other features of charge-density wave transport in the quasi-one-dimensional conductor NbS_3. *Appl. Phys. Lett.* **2009**, *94*, 152112.

(45) van Smaalen, S.; de Boer, J. L.; Meetsma, A.; Graafsma, H.; Sheu, H.-S.; Darovskikh, A.; Coppens, P. Determination of the structural distortions corresponding to the q^1 and q^2-type modulations in niobium triselenide $NbSe_3$. *Phys. Rev. B* **1992**, *45*, 3103–3106.

(46) Schäfer, J.; Rotenberg, E.; Kevan, S. D.; Blaha, P.; Claessen, R.; Thorne, R. E. High-Temperature Symmetry Breaking in the Electronic Band Structure of the Quasi-One-Dimensional Solid $NbSe_3$. *Phys. Rev. Lett.* **2001**, *87*, 196403.

(47) Sambongi, T.; Yamamoto, M.; Tsutsumi, K.; Yamaya, K.; Abe, Y. Superconductivity in One-Dimensional $TaSe_3$. *J. Phys. Soc. Jpn.* **1977**, *42*, 1421–1422.

(48) Haen, P.; Lapierre, P.; Monceau, P.; Núñez Regueiro, M.; Richard, J. Low temperature phase transition in the chain-like compounds $NbSe_3$ and $TaSe_3$. *Solid State Comm.* **1978**, *26*, 725–730.

(49) Fleming, R. M.; Polo, J. A.; Coleman, R. V. Oscillatory magnetotransport in $NbSe_3$ and $TaSe_3$. *Phys. Rev. B* **1978**, *17*, 1634–1644.

(50) Yang, J.; Wang, Y. Q.; Zhang, R. R.; Ma, L.; Liu, W.; Qu, Z.; Zhang, L.; Zhang, S. L.; Tong, W.; Pi, L.; Zhu, W. K.; Zhang, C. J. Observation of charge density wave transition in $TaSe_3$ mesowires. *Appl. Phys. Lett.* **2019**, *115*, 033102.

(51) Stolyarov, M. A.; Liu, G.; Bloodgood, M. A.; Aytan, E.; Jiang, C.; Samnakay, R.; Salguero, T. T.; Nika, D. L.; Rumyantsev, S. L.; Shur, M. S.; Vrozhilov, K. N.; Balandin, A. A. Breakdown curent density in h-BN-capped quasi-1D $TaSe_3$ metallic nanowires: prospects of interconnect applications. *Nanoscale* **2016**, *8*, 15774–15782.

(52) Nie, S.; Xing, L.; Jin, R.; Xie, W.; Wang, Z.; Prinz, F. B. Topological phases in the $TaSe_3$ compound. *Phys. Rev. B* **2018**, *98*, 125143.

(53) Zhang, Y.; Zhu, T.; Bu, H.; Cai, B.; Xi, C.; Chen, B.; Wei, B.; Lin, D.; Xie, H.; Naveed, M.; Xi, X.; Fei, F.; Zhang, H.; Song, F. Large magnetoresistance in topological insulator candidate $TaSe_3$. *AIP Advances* **2020**, *10*, 095314.

(54) Silva-Guillén, J. A.; Canadell, E.; Ordejón, P.; Guinea, F.; Roldán, R. Anisotropic features in the electronic structure of the two-dimensional transition metal trichalcogenide TiS_3: electron doping and plasmons. *2D Mater.* **2017**, *4*, 025085.

(55) Huang, C.; Zhang, E.; Yuan, X.; Wang, W.; Liu, Y.; Chang, C.; Ling, J.; Liu, S.; Xiu, F. Tunable charge density wave in TiS_3 nanoribbons. *Chin. Phys. B* **2017**, *26*, 067302.

(56) Randle, M. et al. Gate-controlled metal-insulator transitions in TiS_3 nanowire field-effect transistors. *ACS Nano* **2019**, *13*, 803–811.

(57) Papadopoulos, N.; Flores, E.; Watanabe, K.; Taniguchi, T.; Ares, J. R.; Sánchez, C.; Ferrer, I. J.; Castellanos-Gómez, A.; Steele, G. T.; van der Zant, H. S. J. Multi-terminal electronic transport in boron nitride encapsulated TiS_3 nanosheets. *2D Mater.* **2020**, *7*, 015009.

(58) Randle, M. A.; Lipatov, A.; Mansaray, I.; Han, J. E.; Sinitskii, A.; Bird, J. P. Collective states and charge density waves in the group IV transition metal trichalcogenides. *Appl. Phys. Lett.* **2021**, *118*, 210502.

(59) Itkis, M. E.; Nad, F. Y.; Levy, F. Energy band structure of the quasi-one-dimensional conductor NbS_3. *Synth. Met.* **1991**, *41-43*, 3969–3972.

(60) Wu, K.; Blei, M.; Bin, C.; Lei, L.; Hui, C.; Brayfield, C.; Wright, D.; Zuang, H.; Tongay, S. Phase Transition Across Anisotropic NbS_3 and Direct Gap Semiconductor TiS_3 at Nominal Titanium Alloying Limit. *Adv.Mater.* **2020**, *32*, 2000018.

(61) Misse, P. R. N.; Berthebaud, D.; Lebedev, O. L.; Maignan, A.; Guilmeau, E. Synthesis and Thermoelectric Properties in the 2D $Ti_{1-x}Nb_xS_3$ Trichalcogenides. *Materials* **2015**, *8*, 2514–2522.

(62) Guilmeau, E.; Berthebaud, D.; Misse, P. R. N.; Hébert, S.; Lebedev, O. L.; Chateigner, D.; Martin, C.; Maignan, A. $ZrSe_3$-Type Variant of TiS_3: Structure and Thermoelectric Properties. *Chem. Mater.* **2014**, *26*, 5585–5591.

(63) Hohenberg, P.; Kohn, W. Inhomogeneous Electron Gas. *Phys. Rev.* **1964**, *136*, B864–B871.

(64) Kohn, W.; Sham, L. J. Self-Consistent Equations Including Exchange and Correlation Effects. *Phys. Rev.* **1965**, *140*, A1133–A1138.

(65) Dovesi, R.; Erba, A.; Orlando, R.; Zicovich-Wilson, C. M.; Civalleri, B.; Maschio, L.; Rerat, M.; Casassa, S.; Baima, J.; Salustro, S.; Kirtman, B. Quantum-mechanical condensed matter simulations with CRYSTAL. *WIREs Comput. Mol. Sci.* **2018**, *8*, e1360.

(66) See `http://www.crystal.unito.it` for details on the CRYSTAL code, Gaussian Basis Sets, Computational schemes, etc., 2019; accessed January 2019.

(67) R. Dovesi, V. R. Saunders, C. Roetti, R. Orlando, C. M. Zicovich-Wilson, F. Pascale, B. Civalleri, K. Doll, N. M. Harrison, I. J. Bush, P. D'Arco, M. Llunell, M. Causà, Y.

Noël, L. Maschio, A. Erba, M. Rerat, S. Casassa, CRYSTAL17, (2017) CRYSTAL17 User's Manual. University of Torino, Torino.

(68) Soler, J. M.; Artacho, E.; Gale, J. D.; García, A.; Junquera, J.; Ordejón, P.; Sánchez-Portal, D. The SIESTA method for ab initio order-N materials simulation. *J. Phys.: Condens. Matt.* **2002**, *14*, 2745–2779.

(69) Artacho, E.; Anglada, E.; Diéguez, O.; Gale, J. D.; García, A.; Junquera, J.; Martin, R. M.; Ordejón, P.; Pruneda, J. M.; Sánchez-Portal, D.; Soler, J. M. The SIESTA method; developments and applicability. *J. Phys.: Condens. Matter.* **2008**, *20*, 064208.

(70) García, A. et al. SIESTA: Recent developments and applications. *J. Chem. Phys.* **2020**, *152*, 204108.

TOC Graphic

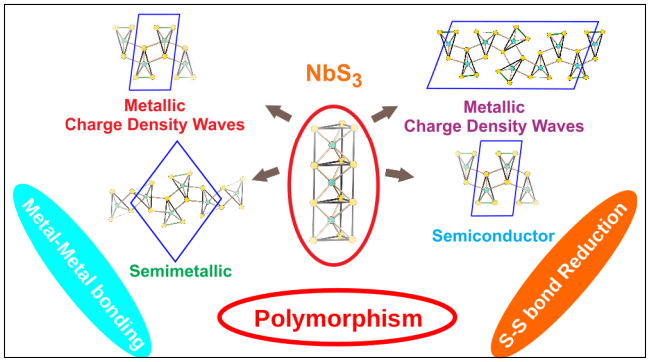
NbS3
Metallic
Charge Density Waves
Metallic
Charge Density Waves
Semimetallic
Semiconductor
Metal-Metal bonding
S-S bond Reduction
Polymorphism